



Cartography M.Sc.

Master thesis

Mapping the Vegetation of the Caucasian Ushba Region (Georgia, Russian Federation) as a contribution to an Alpine Club Map

Michael Hallett



2020

Mapping the Vegetation of the Caucasian Ushba Region (Georgia, Russian Federation) as a contribution to an Alpine Club Map

submitted for the academic degree of Master of Science (M.Sc.)
conducted at the Department of Aerospace and Geodesy
Technical University of Munich

Author: Michael Hallett
Study course: Cartography M.Sc.
Supervisor: *Dr.rer.nat.* Nikolas Prechtel (TUD)
Reviewer: *Dipl.-Ing.* Florian Ledermann (TUW)

Chair of the Thesis
Assessment Board: Prof. Dr. Liqiu Meng

Date of submission: 12.10.2020

Statement of Authorship

Herewith I declare that I am the sole author of the submitted Master's thesis entitled:

“Mapping the Vegetation of the Caucasian Ushba Region (Georgia, Russian Federation) as a contribution to an Alpine Club Map”

I have fully referenced the ideas and work of others, whether published or unpublished. Literal or analogous citations are clearly marked as such.

Dresden, 12/10/2020

Michael Hallett

Abstract

This thesis forms part of a team project to produce an Alpine Club map sheet for the Ushba region in Svaneti, Georgia. The Ushba region spans the border between Georgia and Russia and forms part of the Greater Caucasus mountain range. The area is characterised by high mountains and large, open valleys, which lead to the formation of distinctive vegetation zones of which this thesis aims to classify and represent. Classification was carried out using a mixture of remote-sensed image data and relevant literature. Due to the ongoing Covid-19 pandemic throughout 2020 the practicality of a field trip to take measurements was unfeasible. Therefore, accurate references for training data were sourced online in the form of geotagged photos and high-resolution satellite images. A hierarchical image classification approach using ERDAS IMAGINE software was employed to extract vegetation from non-vegetation components, followed by the classification of individual vegetation classes. Using this method, it was possible to extract 3 separate classes; mixed, high forest stands, Krummholz and Alpine meadow. These classes were further vectorised with an appropriate colour scheme used for representing each vegetation type, that matched the general legend used by other Alpine Club maps. Further visualisations and classifications proved the general trend of vegetation over time both seasonally and over multiple years and established the compatibility between using Landsat-8 and Sentinel-2 satellite imagery. Overall accuracy using the correlation coefficient was proved to be 86% with a Kappa value of 0.78 which suggests the vector layers produced are fit for the purpose of use. It should be mentioned that the reliability of classifications is under question due to the lack of training data from the field, but it is hoped that future studies will correct for this.

Contents

FIGURES	II
TABLES	IV
EQUATIONS	V
1.0 INTRODUCTION	1
1.1 RESEARCH OBJECTIVES	1
1.2 CLIMATE OF THE USHBA REGION	2
1.3 VEGETATION ZONES OF THE USHBA REGION	2
1.4 VEGETATION REPRESENTATION IN THE ALPINE CLUB MAP SERIES	7
1.5 PAST RESEARCH AND THEORY	8
2.1 MULTI-SPECTRAL IMAGES	13
2.2 REFERENCE DATA	16
3.0 METHOD	26
3.1 DATA PRE-PROCESSING	28
3.2 LEVEL 1 VEGETATION CLASSIFICATION AND SEGMENTATION	29
3.3 LEVEL 2 VEGETATION CLASSIFICATION	32
3.4 POST-PROCESSING OF CLASSIFICATIONS	34
4.0 RESULTS AND DISCUSSION	38
4.1 RESULTS OF VEGETATION CLASSIFICATIONS	38
4.2 NDVI ANNUAL TIME SERIES	46
4.3 YEARLY COMPARISONS	49
4.4 SATELLITE COMPARISONS	50
4.5 DISTINCTION OF VEGETATION BOUNDARIES	54
4.6 TIMELINE OF OVERALL CLASSIFICATION	55
4.7 FOREST-TYPE CLASSIFICATION	57
4.8 CONFUSION MATRIX	59
5.0 CONCLUSIONS	60
REFERENCES	62

Figures

Figure 1 - Image examples for high forest stands within the Ushba region.	3
Figure 2 - Image of flowering Caucasian Rhododendron.	4
Figure 3 - Alpine grassland shown with Ushba in the background.	5
Figure 4 - Legend example for the Alpine Club map series.	7
Figure 5 - Map extract from the Alpine Club map of Triglav in the Slovenian Alps.	8
Figure 6 - No. of image scenes taken from each month.	16
Figure 7 - Extract of Russian military map from 1989. Highlighted Circles in red show forest types present.	16
Figure 8 – Map showing the general distribution of training areas across Ushba study area.	17
Figure 9 - The mean spectral signatures of the target vegetation classes ((a) Sentinel-2 and (b) Landsat-8).	19
Figure 10 - Example of stacking bands using the ERDAS IMAGINE software.	26
Figure 11 - Workflow pipeline of the method used in this study.	27
Figure 12 - Spatial subset of stacked Sentinel-2 and Landsat-8 bands to correct map boundary coordinates.	28
Figure 13 - Reprojection of the image stacks and resampling to correct output cell size. Output is also snapped to pixel edges of other stacks.	29
Figure 14 - Spectral profile for the vegetation index of tile 37, landsat-8 scenes.	30
Figure 15 - Example of problematic spectral profile with probable cloud cover appearing in scenes 5 and 9.	31
Figure 16 - Model for removal of cloud cover from individual scenes within the image stack.	31
Figure 17 - Model used to add a threshold to the image scenes removing all non-vegetation from all the images.	32
Figure 18 - Signature editor for the Landsat-8, tile 37 image stack as calculated using ERDAS software.	33
Figure 19 - Supervised classification on ERDAS using the maximum likelihood function and pre-determined signatures.	33
Figure 20 - Recoding of the s38_2 classified image.	35
Figure 21 - Model used to unify the two classifications into a single 3-class product.	35
Figure 22 - Process of vectorising the raster image using tools on ArcMap.	37
Figure 23 - Extract of vegetation and non-vegetation components within the Ushba region. Scale of 1:115,000.	39
Figure 24 - Combined extract of all forest types (dark green) and Alpine meadow (light yellow). Scale of 1:115,000.	40
Figure 25 - Extract of only high forest stands, shown in light green, compared to other vegetation layers (Krummholz and Alpine meadow) which are shown in brown-yellow. Scale of 1:115,000.	41
Figure 26 - Magnified view of the final classification output with contour lines marked. For the full-sized version see figure 5.	42
Figure 27 – Classification output overlaid on top of the Ushba DEM showing contours at 100 metre elevations. Scale of 1:115000.	43

<i>Figure 28 - Final classified product from the best Sentinel-2 scene combinations. Scale of 1:115,000.</i>	45
<i>Figure 29 - NDVI times series for the Sentinel-2 satellite covering the period between April and July.</i>	47
<i>Figure 30 - NDVI times series for the Sentinel-2 satellite covering the period between August and November.</i>	48
<i>Figure 31 - Comparison between the months of different years within the Sentinel-2 image data. Images scenes were chosen based on similar sensing dates.</i>	49
<i>Figure 32 - Comparison between the NDVI classification taken from Landsat-8 (a) and Sentinel-2 (b). Scale of 1:115,000.</i>	51
<i>Figure 33 - Comparison between NDVI classification taken from Sentinel-2 images and Landsat-8 images over the stated months. Image scenes were chosen based on close sensing dates.</i>	52
<i>Figure 34 - Comparison between the classification results of the two satellite image types used in this study. Both at Scale of 1:115,000.</i>	53
<i>Figure 35 - Close view of the vegetation borders resulting from the classifications. Respective image scales from the top to the bottom image are 1:55,000, 1:25,000 and 1:10,000.</i>	54
<i>Figure 36 - Timeline of classification outputs for the Ushba region. All maps are at a scale of 1:115,000.</i>	56
<i>Figure 37 - Classification of the different forest types; coniferous in dark green, deciduous in light green and meadow in light yellow. Map is at the scale of 1:115,000.</i>	58

Tables

<i>Table 1 - Overview of Sentinel-2 and Landsat-8 satellites.</i>	14
<i>Table 2 - Description of the data accessed from each satellite and each tile.</i>	15
<i>Table 3 - Description of training areas.</i>	18
<i>Table 4 - First half of the description of training area references for the Forest Class vegetation.</i>	20
<i>Table 5 - Second half of the references for the Forest Class vegetation.</i>	21
<i>Table 6 - First half of references for the Krummholz vegetation class.</i>	22
<i>Table 7 - Second half of references for the Krummholz vegetation class.</i>	23
<i>Table 8 - First half of references for the Meadow vegetation class.</i>	24
<i>Table 9 - Second half of references for the Meadow vegetation class.</i>	25
<i>Table 10 - Description of the final products derived from the method used in this study.</i>	36
<i>Table 11 - Confusion matrix for the classification based on correct or incorrect classification of training areas.</i>	59

Equations

<i>Equation 1 - Random Forest equation acquired from the study by Vega Isuhuaylas et al. 2018.</i>	<i>11</i>
<i>Equation 2 - Cohen's kappa coefficient.</i>	<i>13</i>
<i>Equation 3 - Normalised Difference Vegetation Index equation.</i>	<i>29</i>
<i>Equation 4 - Maximum likelihood equation (from the study by Richards J. 1999).</i>	<i>34</i>
<i>Equation 5 - Kappa Coefficient.</i>	<i>60</i>

1.0 Introduction

This thesis encompasses a contribution to the Alpine Club map of the Ushba region regarding the mapping of the vegetation zones. The vegetation layer is produced from a combination of remote sensed data, image classification and relevant literature sources. The report shall focus on the identification of the predefined vegetation zones and their extraction from the images of the Landsat-8 and Sentinel-2 satellite missions. Following this a suitable classification of the vegetation zones will be chosen.

Mount Ushba is situated on the Russia-Georgia border within the Greater Caucasus mountain range. The original focus of this thesis was on the Georgian side with subsequent expeditions planned to map across the Russian border, however, due to the Covid-19 pandemic this focus became redundant. The mapping area lies within the Svaneti region of North Western Georgia, a region characterised by high mountains and large valleys. In recent years the area around Mestia, the main town within the Upper Svaneti region, has experienced a rapid increase in tourism (119% from 2017 to 2018 [1]). This increase in tourism is sparked by a recent tourism drive by the government and enhanced by beautiful hiking conditions in the surrounding landscape. A map sheet of this area is considered useful for hikers and general tourists alike.

The Covid-19 pandemic had a number of impacts on this thesis in particular the feasibility of a field trip as well as access to university computer software. These problems had to be overcome in order to successfully meet the outcomes, all of which shall be discussed later in this thesis paper.

1.1 Research Objectives

As previously mentioned, the main research objective is to produce a symbolised layer of actual vegetation cover based on the remotely scanned satellite images. This will be done by answering several research questions:

- How is the vegetation of the Ushba region composed in terms of natural vegetation zones?
- How are the different zones of vegetation related on the slopes of the Ushba mountain range?
- How can these vegetation zones be classified using satellite data (Landsat-8, Sentinel-2)?
- In what way can the vegetation zones be categorised/symbolised according to Alpine Club Map standards?
- How is it possible to characterise the different transitions between vegetation zones (sudden boundary vs. gradual change etc.)?

This thesis covers the expansion of the Alpine Club map series into a new, currently uncovered region which, as previously mentioned, is experiencing an increase in international tourism year on year. This research is to focus mainly on the Georgian side of the Ushba region and will cover

the mapping of the vegetation zones not the ice or rock layers. It is hoped that the vegetation layers from this study will be used in a final version of the map sheet that can be used by mountaineers, hikers and general tourists interested in exploring this region.

1.2 Climate of the Ushba Region

The climate of the Ushba region of Georgia is relatively warm and humid with up to 2200 mm of rainfall per year [2]. Half of this annual precipitation falls as snowfall during the colder months meaning large areas of the mountains are covered by snow for much of the year; depending upon the elevation. Georgia is protected from cold, northern air intrusions by the Greater Caucasus mountain range and an influx of warm, moist air is provided from the direction of the black sea [3]. In the Svaneti region (where Ushba is located) this influence is particularly apparent due to relative proximity to the Black sea. Numerous similarities can be seen between the climate of the Caucasus and that of the Alps as described, in more detail, in studies by Nakhutsrishvili and Körner [2], [4], [5]. Although the two ranges show similarities the Caucasus exhibit a much stronger continental effect and show much sharper climatic variations over relatively small distances [2]. The impact of the humid climate on the Ushba region is to lower the temperature and thereby lower the isotherms in respect to Eastern or further inland regions of the Caucasus. As a result, both the tree line and snow line are lower in comparison.

1.3 Vegetation zones of the Ushba region

The vegetation of the Ushba region is dominated by mesophilic taxa (which concerns organisms that grow in moderate temperature ranges) as influenced by the relatively humid and sheltered climate [3] this region exhibits. Typical Colchis vegetation elements [2] characterise the Svaneti region which refers to the locality (the area of land covering the shores of the black sea and south of the Caucasian mountains). Nakhutsrishvil et al. [2] describe the vegetation in detail; forests made up of coniferous pine trees such as Oriental Spruce, mixed deciduous forest with Oriental Beech canopy and Rhododendron understory. Other species such as Oak, Fir, and Hornbeam are also noted as present within the forest zone according to Berdzenishvili et al. [6]. For a visual example of these species and forest types, see Figure 1 [7]–[9]. At the upper limit the forests give way to Krummholz, an area of stunted wind-blown trees that grow near the canopy [10], which, in the Svaneti Region, are composed of more oriental beech, red bud maple and birch [1]. Nakhutsrishvil et al. goes on to describe that beyond the tree line shrubs are more dominant; in particular, Caucasian Rhododendron and Common Juniper. Higher still, tall herb fields become prolific in the subalpine meadows with both the size and occurrence of plants decreasing with increasing altitude. These vegetation zones are typical for this region and directly affected by altitude and the associated climate.

The tree limit, as identified by Nakhutsrishvil et al. [2], is 2500 metres at its highest and is represented by local patches of low stature, birch trees. This matches the tree line found in other mountain ranges (such as the certain parts of the Alps, Hawaii and the Canadian Rockies [11]–[14]) where the thermal conditions match. The upper limit of pine forest is found not to pass the 11 °C-isotherm during the warmest months of the year [15]. This means the tree line can move, both higher and lower, within the same mountain range depending on the position of this temperature line. Therefore, in locations closer to the sea, such as with Ushba, the relatively wet climate cools the average temperature within the summer months meaning the tree line is lower than comparative elevations further inland. Forest communities within the subalpine belt are mainly restricted to steep slopes due to the impacts of grazing herds and other farming practices [2]. The natural conifer treeline has disappeared and the birch trees only remain because of protection due to their religious significance [2] indicating significant levels of hemeroby [16]. This makes the

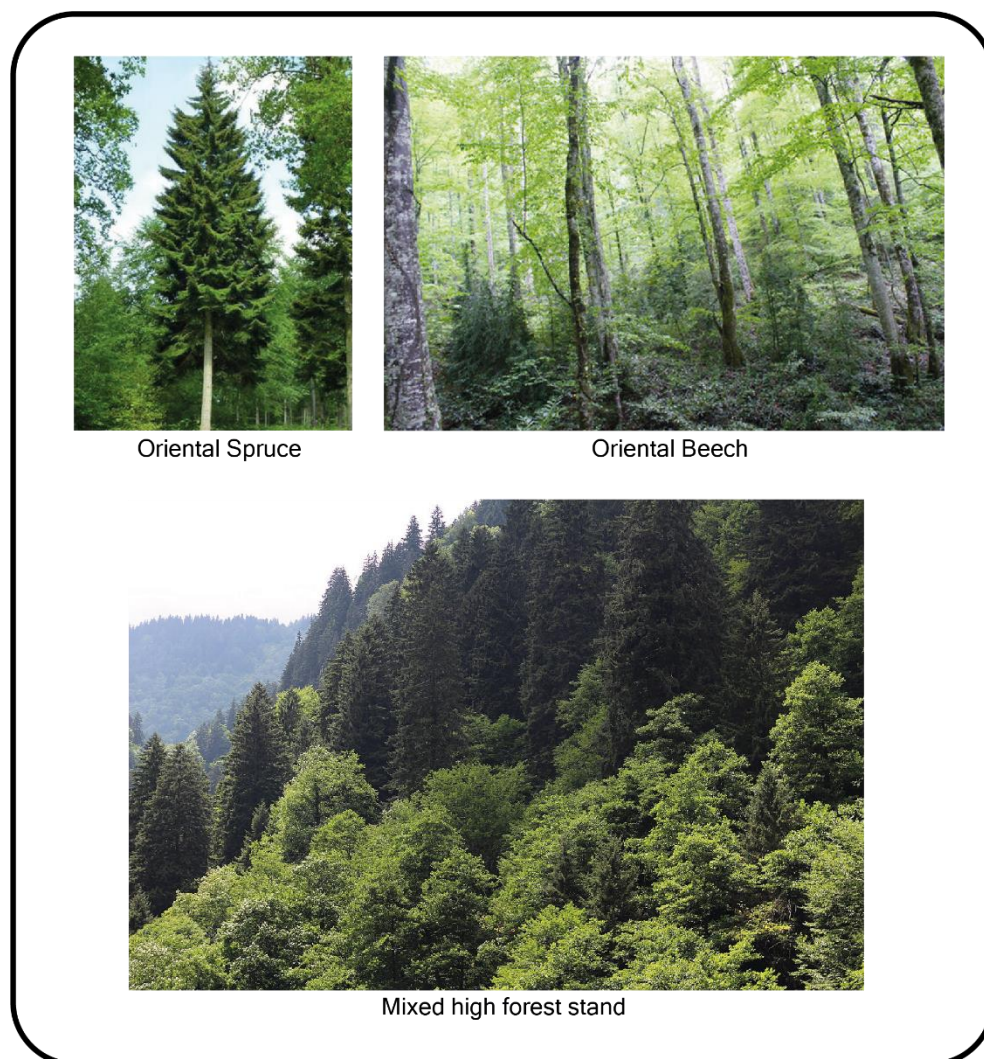


Figure 1 - Image examples for high forest stands within the Ushba region.

mapping of a boundary between different vegetation zones harder as the boundary is often neither straight nor distinct. The tree line is highlighted by high levels of plant diversity and the

majority of wood species are found to be endemic to the Caucasus and neighbouring mountains [2]. However, many species show similarities to those found in the mountain ranges in other parts of Europe (the Alps and Scandinavia) [17].

The subalpine belt is recognised as having been under pressure from the grazing of both wild and farmed animals for many years which have shaped the vegetation zones and their extent today [2]. Tortuous stemmed birch forests (Krummholz) are formed in two ways; the weight of snow in winter pushes down on their stems and results in an elfin form and exposure to strong mountain winds which results in their crooked stem appearance [2], [18]. These attributes mark their position at the higher limit of the subalpine belt between 2350-2550 metres in elevation [2]. Usually accompanying or coexisting with the Krummholz is the Caucasian Rhododendron (see Figure 2 [19]) which is the dominant species in snow cover dependent ecosystems [2]. This allows the species to form dense coverage of nearly 100% in the subalpine regions between 2300-2900 metres elevation. Rather than a continuous layer, the location of these thickets, will exist sporadically depending on local environmental conditions. These two species will constitute the 'Krummholz' map layer which will exist between the mixed woodland previously mentioned and the forb and grass communities which will be mentioned in subsequent paragraphs.

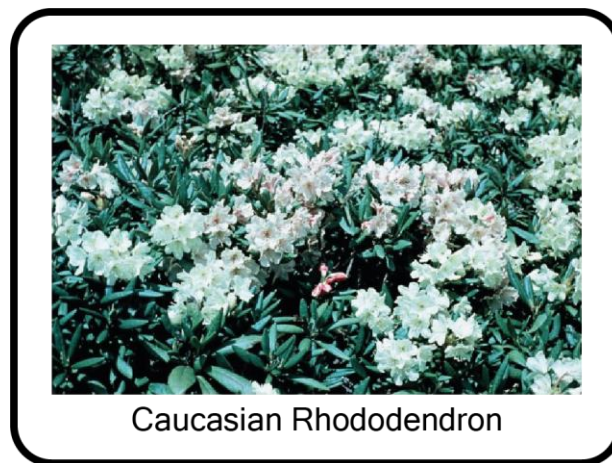


Figure 2 - Image of flowering Caucasian Rhododendron.

The tall herbs of the Caucasus are described in a number of studies [20]–[22] due to their height (between 100-300 centimetres [2]), relative abundance and diversity. The majority of the species, 62% according to Nakhutsrishvil et al. [2], are considered endemic. These tall herb species are all characterised by rapid spring growth to make the most of short summers relying on high air humidity and soil moisture to propagate their growth. They are found at altitudes of around 1900-2300 metres where fluctuations of daily temperature remain moderate [2]. The subalpine meadows can occupy anywhere within the subalpine belt between 1500-2500 metres depending upon the species. Nakhutsrishvil [2], [4] describes them as mesic habitats, meaning that they have access to a moderate water supply, provided by the existing humid conditions in this part of the Caucasus. The subalpine meadows are not natural in formation but rather formed by mowing or

grazing and often make up either hayfields or pastures representing further hemeroby [16]. The alpine meadows can be split into two classes: Tussocky and non-Tussocky grassland. These are represented by differences in both their appearance and species present but would be considered a single entity on the proposed map. Tragacanthic and herb communities occur sporadically throughout the subalpine belt with the latter occurring in depressions and valleys where there is more moisture present [2]. Tragacanthic species occur in areas once occupied by pine forest and include grasses and dwarf shrubs. As the coverage of these areas is so small, they will be considered as an extension of the subalpine meadows layer on the map. Several other vegetation communities of insignificant extent are recognised by Nakhutsrishvil et al. [2] as growing within the subalpine region, these include; rock and scree, Ephemeroid and Phenorythm-type species.

Above the tree line and into the Alpine belt of the Caucasus the dominance of Krummholz and Rhododendron thickets is replaced by Alpine grassland and other short-stature vegetation. Alpine grasslands occupy vast areas and are often used for grazing by cattle, sheep or goats. The Alpine grasslands are made up of a few different communities including sedge grasslands, herb fields and tussocks [2]. Alpine grasses often occupy the steepest and most exposed slopes where larger plant species are unable to grow. Meadow species associated with the alpine region can be found anywhere between 1500-3000 metres. Alpine grasses form carpet-like meadows over vast areas of relatively deep and peaty soils (see Figure 3 [23]). In the highest regions of the Alpine belt snow cover can last up to three quarters of the year therefore plant communities here have to adapt to survive in these extremes. Snowbed communities are found at elevations near to or above 3000 metres. They are mainly composed of low stature forb species with low floristic richness. Despite similarities in species present seen between other mountain ranges and Caucasus lower down within the subalpine belt, several studies have shown that Snowbed communities here are distinct



Alpine Grassland

Figure 3 - Alpine grassland shown with Ushba in the background.

from Snowbed communities seen in other mountain ranges [2] (particularly the Anatolian Mountains in Turkey [24], [25]). Low-stature Caucasian *Rhododendron* shrubs occupy steep gullies between the 2300-3000 metre elevations. Here they are protected by long and secure snow cover within the peri-glacial region [26] providing high humidity and peaty soils. Dwarf shrubs such as *Dryas* occupy stony slopes within the Alpine region mixing with other Alpine Rock and Scree vegetation. These plant communities will all form the proposed Alpine grassland and forb layer on the Ushba map.

The final vegetation community ascending 3000 metres above sea level is described as the Subnival layer. This zone occupies the region between the alpine grasslands and the permanent snow line and glaciers. Life for plants at this altitude is extremely tough and snow cover can often last throughout the year with short, cold summers dominated by long winters [2]. Wind, inclination of slopes, direction of slope face, and surface roughness all have an impact on plant communities that survive here [5], [27], [28]. Most Subnival plants exist in microclimates where they form cushion or carpet-like stands that are warmer than the outside temperature [2]. However others grow as isolated individuals or within small groups sheltering amongst areas of rock and scree [29]. According to Körner et al. [5] the substrate, nutrient and water availability are all shaped by the actions of gravity and thus control the geodiversity of the Subnival belt. Therefore the majority of plant species survive within individual microclimates (ecological niches) and are consequently endemic to the Caucasus range [4] with specific substrate preferences [30]. Nakhutsrishvil et al. [2] even noted 94 species as living above the snowline within the Svaneti region. The subnival layer is difficult to map due to its patchy coverage intermixed with rock and snow therefore further observation through remote sensing and field observations are required to fully map this zone.

From reviewing the literature, it is apparent there is a possibility of identifying three or four vegetation zones seen both on the ground and through remote sensing. Mixed deciduous woodland, Krummholz, and Alpine grassland and herbs make up the most visible layers with a subnival layer likely sporadic in appearance and more difficult to identify using image classification techniques. Based on literature many smaller vegetation classes appear present within the Ushba region but for purposes of this study these smaller plant communities shall be grouped together into the three larger vegetation zones. The primary importance of vegetation representation for the proposed Ushba hiking map is zonation. This allows hikers and other users the ability to see how changes in elevation are represented by the changing vegetation around them and therefore exact marking of each species is unnecessary.

1.4 Vegetation Representation in the Alpine Club Map Series

The Alpine club maps series has no established legend or common classification scheme. This is due to the differences, in vegetation zones present and coverage of vegetation, across the diverse locations which Alpine Club maps are offered. Alpine club maps are praised on their level of accuracy and terrain detail but from observing multiple series maps the number of vegetation zones are usually kept to a minimum. This prevents the maps from becoming too confusing and thus more difficult to read and interpret. An example of an Alpine Club map is shown in Figure 5 [31]. From this figure it is clear to see how the forest on the lower slopes (around the edges of the map) leads up into the rocky areas at higher ground. Here there is some differentiation of the forest; between Krummholz and high forest stands, where patchy darker green elements are shown at the forest fringes. In other Alpine Club map examples; such as Dachstein, the vegetation is clearly split into two types including small pine and bushes (Krummholz), and forest (see Figure 4 [32]). The simple vegetation scheme clearly shows the reader the zonation of vegetation coverage without making it the focus of the map. Other map elements such as the presence of rocky areas, contours and, of course, the hiking trails themselves are prioritised so that the vegetation merely acts as a background layer or base map.



Figure 4 - Legend example for the Alpine Club map series.

Boundaries between vegetation zones are distinctive and show exact changes from one vegetation type to another. This is likely not occurring on the ground, but this representation provides the reader with an idea of where they should see the vegetation zones begin to change. Figure 5 provides a good example of how vegetation boundaries are not always so precise; some forest and Krummholz occur simultaneously with some Krummholz present within the forest zone and both areas of forest and Krummholz cohabitating the upper limits of the tree line. Therefore, although the boundaries between the two vegetation layers are hard, the visualisation shown within Alpine Club maps clearly represents a close interpretation of what is occurring within the natural environment. This shall be considered when deciding on the vegetation layer boundaries within this thesis study.

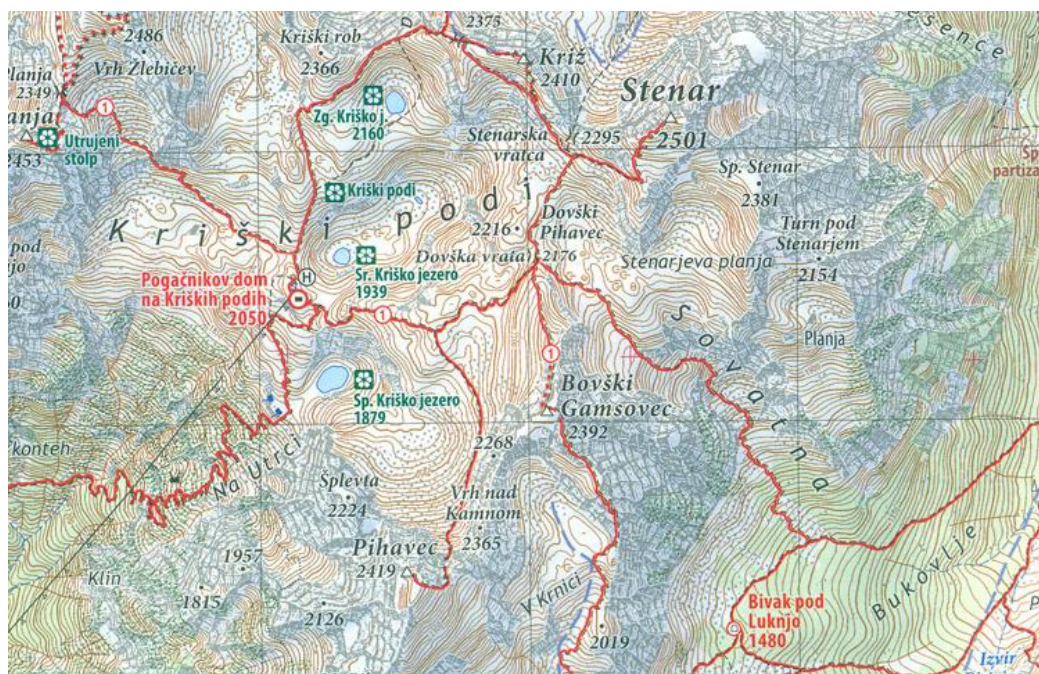


Figure 5 - Map extract from the Alpine Club map of Triglav in the Slovenian Alps.

1.5 Past Research and Theory

Many studies note the difficulty in modelling the vegetation characteristics in high-altitude environments. Characterised by a shorter growing season and long cold winters, as previously mentioned in chapter 1.2, the opportunity to reliably and accurately classify vegetation, based on NDVI in these regions, is limited [33], [34]. Parallels can be drawn with the quantification of the vegetation index at high-latitude regions as in the study by Beck et al. [35]. In this study a Moderate Resolution Imaging Spectroradiometer (MODIS) NDVI is used instead of the typical NDVI time series due to its better performance within such latitudes. The importance of observing the winter time series as well as the typical leaf-on period between March and October is highlighted in several studies [35]–[37] and the relevance of snow cover in regards to its impact on mountain phenology is highlighted in many more [38]–[40]. In a detailed study on the impact of snow, Xie et al. [41] measured the impact of snow accumulation and duration on mountain phenology and concluded that snow cover duration had the most impact on the timings and behaviour of vegetation as a whole. Previous research promotes the importance of considering the snow cover during a study of vegetation within high mountain regions [36], [42]. Although this study is primarily focused on arriving at a vegetation classification and not analysing phenology it is a point of consideration for the methodology and the practical aspect of arriving at an accurate classification product.

Three problems with accurately mapping the vegetation zones using mid-resolution satellites such as Landsat-8 are described in the study by Cingolani A. et al. [43]. One such problem is the

presence of vegetation community patches which are smaller than the pixel size of the Landsat image and thus difficult to reliably classify [44]. The study suggests the approach of defining informational units at a higher hierarchy (where classes are defined by terrain attributes) to give a more realistic classification product [45]. Another problem focussing in the study by Cingolani et al. [43] is the definition of exact mapping units that are discernible by the satellite itself. It is noted that a process of trial and error occurs until a satisfactory output is produced [44]. This is realised within the Ushba region by the presence of several smaller plant communities which are mentioned within literature but would be indiscernible by a satellite classification. Thus, a suitable number of classes and training areas must be used to best represent a classification and output that is appropriate for an Alpine Field Club map. This then leads to the third problem of perceiving suitable training areas of adequate size. In the paper mentioned [43], an objective method of selecting training sites and assigning pixels based on discriminant functions is suggested. These discriminant functions are obtained from the statistical analysis of the spectral signatures of each vegetation class which subjected each pixel to eight linear functions (for each band of the Landsat TM satellite). Each of these 8 values were subsequently compared followed by the assignment of the pixel to the class with the highest value [43]. This method resulted in a relatively high accuracy (~87%) but for this study the problem lies with a lack of reliable field data to give accurate spectral comparisons. Therefore, it would not be feasible to use this method for the classification of vegetation in the Ushba region.

Airborne multispectral imagery has been used as a source for vegetation and water remote sensing since the 1960s [46]. This type of imagery is limited in the number of bands that it can measure thus limiting the spectral resolution of multispectral satellite imaging. In the study by Govender et al. [47] the use of hyperspectral remote sensing is described as the answer to these limitations. Hyperspectral sensors measure continuous spectral bands as opposed to multispectral imaging which measure spaced spectral bands [48]. Hyperspectral sensors can collect up to 200 bands allowing for the complete reconstruction of a contiguous reflectance spectrum for every pixel in an image [47]. This can then be used to produce a more detailed analysis of surface cover with finer discrimination between different classes arriving at a more accurate or detailed classification. Although the spectral resolution of the hyperspectral sensor is higher the spatial resolution is not. This is due to the differences between spectral and spatial resolution: Spectral resolution is referring to the number and width of electromagnetic spectrums whereas spatial resolution refers to the level of spatial detail that can be visualised [47]. This is very relevant to this thesis as an application of hyperspectral sensing is the discrimination of different vegetation types something which is possible with multispectral sensors (such as Sentinel-2 and Landsat-8) but not as accurate.

The most important part of the methodology for this thesis is the implementation of the classification. Many different classification methods are discussed throughout different studies focussing on the pre-processing or different classification techniques available. In the study by Iovan et al. [49] the different variances of grass and trees is used to separate and individually classify the two surface types. Other studies describe detailed pre-processing in order to remove

noise and make images homogenous in appearance [41], [50]. Xie et al. [41] remarks that the pre-processing of images usually compromises a series of operations including but not limited to; image enhancement, mosaicking, radiometric correction, geometric correction and masking. The use of masking is particularly important regarding the removal of cloud cover from images. The Ushba image scenes used in this study were chosen based on the least amount of cloud cover but even a small amount of cloud cover present can drastically affect the classification results. The study by Xue et al. [51] describes in detail the use of specific Vegetation Index (VI) algorithms in terms of their application and target vegetation classes. The VI used in most studies is the Normalized Difference Vegetation Index (NDVI) which is the primary method of extracting vegetation using unsupervised classification techniques and the technique that will be used in this study. Most studies make use of the NDVI classification technique to extract the vegetation and then use a more precise supervised classification method to extract the individual vegetation types [50], [52], [53]. In the study by Vanonchelen et al. [53] the Maximum Likelihood (ML) and Support Vector Machine (SVM) classifiers were used. Both classifiers are examples of supervised classification techniques which require the input of training data. For the study mentioned [53], the SVM classifier works by identifying a hyperplane that separates the classes in feature space [54], [55]. This hyperplane maximises the difference along class boundaries and is found to outperform other classification techniques whilst demanding fewer training sites [56]–[60]. However, in order to execute this type of classification the correct level of software is required. In this study by Vanonchelen et al. [53] as well as most of the others mentioned the established ENVI/IDL software was used. In this paper, due to university access constraints, the only software available was ERDAS IMAGINE and SNAP neither of which have the availability of functions that ENVI software allows.

In several past studies the main classifier used was the Random Forest (RF) classifier [50], [61]. The primary function of this classifier type is to extract individual forest or vegetation types, for example; in the study by Liu et al. [50] different tree species were classified from Sentinel-2 and Landsat-8 data sources. RF along with the k-Nearest Neighbour (kNN) algorithm and the SVM classifier, which was mentioned in the previous paragraph, are examples of Machine Learning Algorithms (MLAs). MLAs are useful for classifying vegetation in mountainous regions because there is no need to assume the data is distributed normally. This means that these classifiers can deal with noisy training data and produce more accurate classifications in complex environments [53], [62]. Lu and Weng [62] mention that non-parametric classifiers, such as MLAs, do not require assumptions about the data. This is in reverse to parametric classifiers, such as Maximum Likelihood, which assume a Gaussian distribution and rely mainly on training data in order to arrive at a successful classification. This highlights the benefit of MLAs which can incorporate non-remote sensing data into the classification process. Therefore a reduced reliance on training data is required and resulting classifications appear less ‘noisy’ than parametric classifications of the same area [62]. RF classification consists of a collection of tree-structured classifiers in which

each tree contributes a vote to determine the most frequent class according to the input data (see Equation 1) [61], [63].

$$C_{rf}^m(x) = \text{majority vote}\{C_{m_i}(x)\}_1^m,$$

*Equation 1 - Random Forest equation
acquired from the study by Vega Isuhuaylas
et al. 2018.*

To form a split point node the algorithm randomly selects a sub-set of variables and then searches among these variables to arrive at the best classification boundary between classes [63]. The algorithm performance is limited by the number of tree-structured classifiers. Often other non-remote sensed data must be added when classifying trees with similar spectral signatures. In the study by Liu et al. [50] topographic and phenology information was added into the algorithm in order to distinguish between individual tree species.

Support Vector Machine (SVM) is used in multiple studies [53], [57]–[59], [64], [65] and represents an example of a non-parametric, supervised classification technique. As mentioned in previous paragraphs, SVM works by finding a hyperplane which optimises the classification by minimising the upper classification boundary [61]. The hyperplane surface is used to determine the classification and arrives from the input variables including training data and other non-remote sensed components. In the paper by Cortes and Vapnik [64] the use of soft margins within the MLA allow for errors within the training data. This is useful for regions of complex vegetation coverage such as those found in mountain environments. In the study by Vega Isuhuaylas et al. [61], SVM was found to outperform other MLA, including RF, when classifying the Andes mountain environment. It was found to have the highest mean area under the curve (AUC) as well as the smallest standard deviation [61] when compared to the poorest performing classification technique. There were differences found between the performance of the SVM using different input data; for example, using NDVI as the only classification feature for SVM severely limited its performance capability. Thus, the main benefit of MLAs is once again highlighted by their ability to acknowledge other data features including phenology, topography and elevation data. The overall benefits of SVM as a classifier is evident by its ability to deal with noisy training data in complex environments. Therefore, it would be a useful classification technique for mapping the vegetation of Ushba.

The final non-parametric technique evaluated in the study by Vega Isuhuaylas et al. [61] and used in a variety of studies in order to classify forest environments [66]–[68] is the k-Nearest Neighbours (kNN) classification algorithm. This technique is simple to implement; requires low training data, computational costs and relies on the k-closest training data vectors in order to compute accurate classifications. The kNN classification works by assigning a sample vector 'x' to the class represented by the majority of 'k' nearest neighbours [61]. The value of the point variable is predicted based on the similarity between neighbouring points that show observed values within a covariate space [68]. Similarity between the nearest neighbour values is determined by distance but as with all non-parametric MLAs other variables can be included in the overall

calculation. In terms of performance, the kNN classification method has many good performance indicators when used in forestry mapping. Attention must be paid when calibrating the kNN classification technique as noted by McRoberts et al. [68]. By weighting some variables more than others it was found that the accuracy of the classification could be increased. However, in the study by Vega Isuhuaylas et al. [61], kNN was found to have a much lower performance when mapping vegetation with noisy, multivariate datasets in comparison to other MLA classifiers such as RF and SVM. This was concluded to be a result of the sensitivity of the kNN classifier to noisy data, in particular - outliers, which could have a large impact on the differences in similarity which the algorithm relies upon. Therefore, it has been concluded that, in comparison to other classifiers, kNN is maybe not as reliable especially regarding the mapping of more complex and challenging environments such as mountainous regions.

The three non-parametric or Machine Learning Algorithms (MLA) mentioned in the last few chapters all have positive and negative features that make them suitable or unsuitable for use in mapping a mountainous region such as Ushba. The main issue with these methods is whether they are supported on the software available for use at TU Dresden (2016 version or ERDAS IMAGINE). Another issue is the lack of reliable training data which is accessible to us due to the cancellation of the planned field trip in July. For these reasons the application of these classification techniques within this study seems unattainable and therefore the supervised classification technique Maximum Likelihood (ML) is to be used instead. ML is the principal parametric classification technique, supported by all image processing software, and the most widely used of all supervised classification techniques [69], [70]. Maximum Likelihood assumes that the statistics for each class are normally distributed in a linear manor. It is therefore assumed that image pixel data follows a Gaussian distribution which is something that is often not true of more complex regions. Each pixel is assigned to a given class based on the highest probability (maximum likelihood) that the pixel belongs to that class based on similarities in the input variables (e.g. NDVI). ML requires sufficient ground truth data in order to arrive at a classification of acceptable accuracy. A greater number of training areas provide a more accurate estimation of the mean vector and variance-covariance matrix of the population. This subsequently arrives at a more accurate classification. Several studies do show that the ML method has its issues and produce less accurate results, particularly in heterogenous mountain environments, when compared to other classification techniques. [43], [52], [61]. However, the study by Sisodia et al. [71] proved ML to be a robust technique; obtaining classification accuracies of 93.75%.

As the last few paragraphs have shown, there is a wide array of possible classification techniques available, all of which can compute sufficient results. One of the most important parts of the method when carrying out a classification of remote sensed data is the ability to check the accuracy of the results. Literature shows that there are several popular methods to compare the classifications by checking the overall accuracy. One such method is the use of Cohen's kappa statistic. Cohen's kappa is defined below (see Equation 2):

$$\kappa = \frac{p_o - p_e}{1 - p_e} = 1 - \frac{1 - p_o}{1 - p_e},$$

Equation 2 - Cohen's kappa coefficient.

where P_o is the observed agreement and P_e is the expected agreement [72]. Resulting values are between 0 and 1 with any value greater than 0.8 being considered as an almost perfect agreement. Generally, the kappa value can be calculated using a confusion matrix which compares the number of correctly classified classes with the number of misclassified classes. Using a confusion matrix; the user, producer and overall accuracy of a dataset can be calculated. Cohen's kappa is a useful tool for measuring multi-class and imbalanced class problems. Another performance indicator used for classification accuracy is the area under the curve (AUC). This was used in the study by Vega Isuhuaylas et al. [61] who used the receiving operating characteristic (ROC) theory to determine the corresponding optimum threshold for each classification analysis. The AUC value, calculated in this way, is threshold independent meaning that the result of this indicator is an overall accuracy based on a number of different probability thresholds [61], [73]. In his study, Friedman [74] employs the use of ranks to check that the variance between different performance indicators is statistically agreeable. From the results of the kappa coefficient and AUC the different classifications can be ranked (1,2,3 etc.) and subsequently these ranks can be compared either pairwise or across all rank classes. In the study by Vega Isuhuaylas et al. [61], the ranks were compared using the Nemenyi post-hoc test which examined whether models showed a notable difference ('Critical Difference'). In conclusion, past research shows how all classification studies must check the overall accuracy of their classification results. The most popular and widely used method is Cohen's kappa but other methods are available and it is preferred to use more than one performance indicator in order to get the most precise accuracy assessments [52], [61], [62]. This is due to, and especially regarding vegetation mapping at coarse scales [52], Cohen's kappa masking errors of significant difference and making the possibility of agreement as a result of chance [75].

2. Data Acquisition

2.1 Multi-Spectral Images

The Multi-Spectral Images (MSI) used in this study are from the Sentinel-2 and Landsat-8 satellite missions. A brief overview of the satellite data used is shown in Table 1.

Satellite	No. of Bands	Spatial Resolution (metres)	Orbit Type	Temporal Resolution (days)	Product Type
Sentinel-2A	13	10 / 20 / 60	Polar	10	Level 1C and Level 2A
Landsat-8	11	30 / 15	Near-Polar	16	Level 1 - Terrain precision Correction

Table 1 - Overview of Sentinel-2 and Landsat-8 satellites.

The Multi-Spectral Sentinel-2 images are made of a satellite constellation of two identical satellites; Sentinel-2A and Sentinel-2B. The Sentinel-2A satellite was launched on the 23rd of June 2015 by the European Space Agency (ESA) and the Sentinel-2B was launched on the 7th of March 2017 [76]. The frequency revisit of each satellite is 10 days with a combined constellation revisit of 5 days at the equator and 2-3 days at mid-latitudes. The two satellites exhibit a polar orbit synchronising the movements of the sun [76]. The instrument consists of a Multispectral Imager (MSI) covering 13 spectral bands (443 nm – 2190 nm) with swath width of 290 km and spatial resolutions of 10 metres (4 visible and near-infrared bands), 20 metres (6 red-edge/shortwave-infrared bands) and 60 metres (3 atmospheric correction bands) [77].

The Landsat-8 satellite was launched on the 11th of February 2013 and includes both the Operational Land Imager (OLI) and the Thermal Infrared Sensor (TIRS) onboard [50]. These two sensors provide seasonal coverage of the global landmass at spatial resolutions of 30 metres (Visible, NIR and SWIR), 100 metres (thermal) and 15 metres (panchromatic) [78].

The MSI used within this study are composed of 64 cropped images taken from both satellites covering the leaf-on period between April and November over the past 3 years (2017-present). Dates were chosen based on percentage cloud cover and in particular; cloud cover over the study area, with less than 20% cloud cover considered acceptable. Sentinel-2 images for 2018/9 were freely acquired from the Copernicus Open Access Hub (<https://scihub.copernicus.eu/>). However, due to the length of time taken to access some of the older archived data using this hub, ONDA (<https://www.onda-dias.eu/cms/>) was used to access all of the 2017 archived data. Resulting products are either Level-1C (L1C) or Level-2A (L2A). L1C describes product images that display top-of-atmosphere reflectances whereas L2A are bottom-of-atmosphere and are derived from the L1C products. L2A tiles are most useful for this study as they provide a clearer image of the ground geometry and vegetation coverage. Therefore, these data types were preferentially chosen where possible (subject to cloud cover and dates). All sentinel-2 products are released in a Universal Transverse Mercator (UTM) projection and World Geodetic System (WGS) 84 datum. A total of 31 tiles were collected with 17 from tile 37 and 14 from tile 38. A description of these images is available in Table 2.

Landsat-8 images were accessed using the USGS Earth Explorer site (<https://earthexplorer.usgs.gov/>) which provides standard Level-1 topographically corrected

products (LT1). LT1 data is corrected with regards to relief displacement. Landsat-8 products are released with a UTM projection and a Clarke 1866 datum. In total 33 Landsat-8 tiles were obtained, 16 for tile 37 and 17 for tile 38. Table 2 provides a description of these images.

SATELLITE	LEVEL	DATE	ERDAS IDENTIFIER
SENTINEL-2A	L2A	17/06/2017	S2_20170617
SENTINEL-2A	L2A	27/07/2017	S2_20170727
SENTINEL-2A	L2A	06/08/2017	S2_20170806
SENTINEL-2A	L2A	06/08/2017	S2_20170806
SENTINEL-2A	L2A	05/09/2017	S2_20170905
SENTINEL-2A	L2A	05/09/2017	S2_20170905
SENTINEL-2A	L2A	12/09/2017	S2_20170912
SENTINEL-2A	L2A	15/09/2017	S2_20170915
SENTINEL-2A	L2A	29/06/2018	S2_20180629
SENTINEL-2A	L2A	28/08/2018	S2_20180828
SENTINEL-2B	L2A	05/09/2018	S2_20180905
SENTINEL-2B	L2A	25/09/2018	S2_20180925
SENTINEL-2B	L1C	29/07/2019	S2_20190729
SENTINEL-2A	L2A	16/08/2019	S2_20190816
SENTINEL-2A	L2A	23/08/2019	S2_20190823
SENTINEL-2B	L2A	30/09/2019	S2_20190930
SENTINEL-2A	L2A	05/10/2019	S2_20191005
SENTINEL-2B	L2A	10/10/2019	S2_20191010
SENTINEL-2A	L2A	20/10/2019	S2_20191020

SATELLITE	LEVEL	DATE	ERDAS IDENTIFIER
SENTINEL-2A	L2A	03/08/2017	S2_20170803
SENTINEL-2A	L2A	12/09/2017	S2_20170912
SENTINEL-2A	L2A	29/06/2018	S2_20180629
SENTINEL-2A	L2A	28/08/2018	S2_20180828
SENTINEL-2A	L2A	05/09/2018	S2_20180905
SENTINEL-2A	L2A	25/09/2018	S2_20180925
SENTINEL-2A	L2A	30/05/2019	S2_20190530
SENTINEL-2A	L2A	09/06/2019	S2_20190609
SENTINEL-2A	L2A	29/07/2019	S2_20190729
SENTINEL-2A	L2A	23/08/2019	S2_20190823
SENTINEL-2B	L2A	02/10/2019	S2_20191002
SENTINEL-2B	L2A	17/10/2019	S2_20191017
SENTINEL-2B	L1C	22/10/2019	S2_20191022
SENTINEL-2A	L2A	06/11/2019	S2_20191106

SATELLITE	LEVEL	DATE	ERDAS IDENTIFIER
LANDSAT-8	L1TP	12/04/2017	L8_20170412
LANDSAT-8	L1TP	28/04/2017	L8_20170428
LANDSAT-8	L1TP	30/05/2017	L8_20170530
LANDSAT-8	L1TP	01/07/2017	L8_20170701
LANDSAT-8	L1TP	02/08/2017	L8_20170802
LANDSAT-8	L1TP	19/09/2017	L8_20170919
LANDSAT-8	L1TP	05/10/2017	L8_20171005
LANDSAT-8	L1TP	01/05/2018	L8_20180501
LANDSAT-8	L1TP	17/05/2018	L8_20180517
LANDSAT-8	L1TP	21/08/2018	L8_20180821
LANDSAT-8	L1TP	22/09/2018	L8_20180922
LANDSAT-8	L1TP	08/10/2018	L8_20181008
LANDSAT-8	L1TP	25/11/2018	L8_20181125
LANDSAT-8	L1TP	08/08/2019	L8_20190808
LANDSAT-8	L1TP	13/11/2019	L8_20191113
LANDSAT-8	L1TP	07/06/2020	L8_20200607

SATELLITE	LEVEL	DATE	ERDAS IDENTIFIER
LANDSAT-8	L1TP	24/06/2017	L8_20170624
LANDSAT-8	L1TP	26/07/2017	L8_20170726
LANDSAT-8	L1TP	11/08/2017	L8_20170811
LANDSAT-8	L1TP	15/11/2017	L8_20171115
LANDSAT-8	L1TP	17/06/2018	L8_20180617
LANDSAT-8	L1TP	27/06/2018	L8_20180627
LANDSAT-8	L1TP	29/07/2018	L8_20180729
LANDSAT-8	L1TP	16/08/2018	L8_20180816
LANDSAT-8	L1TP	01/10/2018	L8_20181001
LANDSAT-8	L1TP	17/10/2018	L8_20181017
LANDSAT-8	L1TP	27/04/2019	L8_20190427
LANDSAT-8	L1TP	29/05/2019	L8_20190529
LANDSAT-8	L1TP	18/09/2019	L8_20190918
LANDSAT-8	L1TP	20/10/2019	L8_20191020
LANDSAT-8	L1TP	13/04/2020	L8_20200413
LANDSAT-8	L1TP	29/04/2020	L8_20200429
LANDSAT-8	L1TP	18/07/2020	L8_20200718

Table 2 - Description of the data accessed from each satellite and each tile.

Figure 6 shows the distribution of Ushba scenes taken from the 2017 - 2020 period. As previously mentioned, scenes were chosen based on cloud cover, but August, September and October were chosen particularly because they have the least amount of snow cover and highest mean NDVI values. Overall, the distribution of scenes were kept as even as possible with an average of 8 scenes per month and an average of 20 scenes for each year (excluding the current year – 2020).

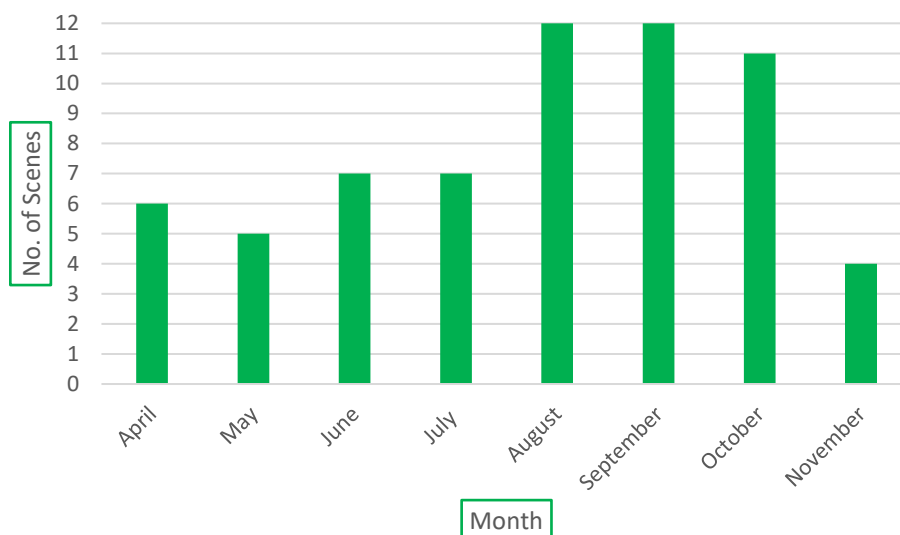


Figure 6 - No. of image scenes taken from each month.

2.2 Reference Data

The collection of reference data for this study was unfortunately affected by the Covid-19 pandemic resulting in the cancellation of a planned trip to the Ushba region for July 2020. This meant that accurate measurements of vegetation zones in the field could not take place. To mitigate this lack of field measurements, reference data was instead obtained using high resolution satellite imagery such as Bing and Google maps. Accompanying this satellite imagery, geotagged photos posted on to google maps were used to identify which vegetation zones a certain photo 'hotspot' lay within. Areas of reference data were chosen as 20x20 pixel blocks of homogenous vegetation. To check areas matched the average NDVI value of the pixels could be calculated using SNAP and ERDAS imagine with matching NDVI values confirming that a training area is concerned of that vegetation type. As well as the use of high-resolution satellite

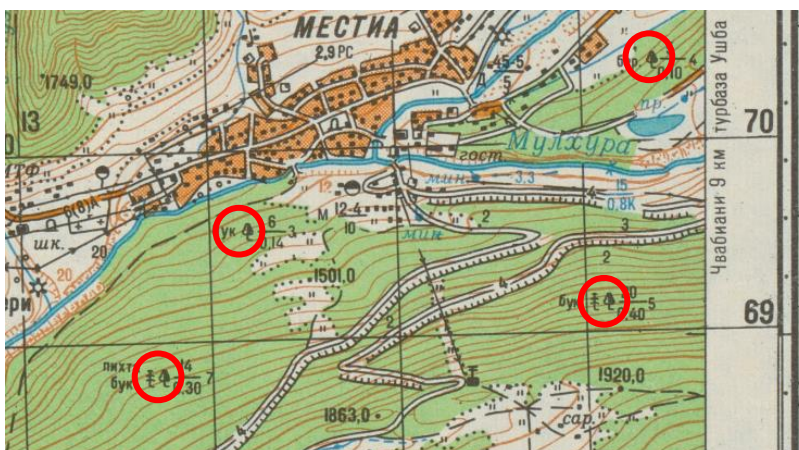


Figure 7 - Extract of Russian military map from 1989. Highlighted Circles in red show forest types present.

imagery, old Russian military maps can be used to identify the type of forest and its presence or absence. In Figure 7 the different forest types are represented by symbols on the map. These can be used to give a clue as to whether an area lies within a deciduous, coniferous or mixed forest stand. However, in the case of this study, classification of forest was grouped into single high forest stands of mixed tree species. This was due to difficulties identifying purely homogenous areas of deciduous or coniferous forest stand from satellite imagery. Furthermore, it was considered unnecessary to separate individual forest types for this category of hiking map based on Alpine Field Club maps of other regions and other hiking maps of the Ushba region.

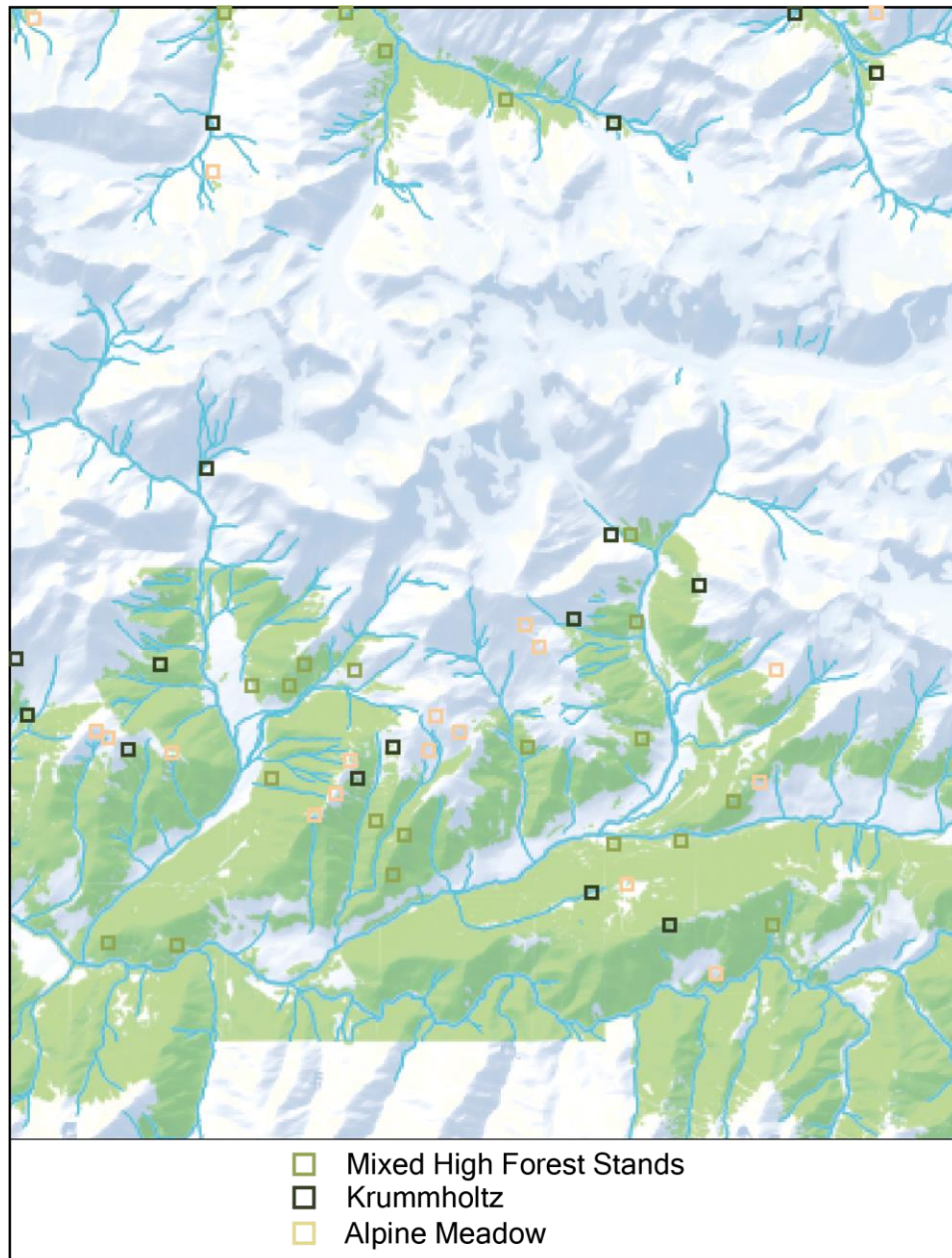


Figure 8 – Map showing the general distribution of training areas across Ushba study area.

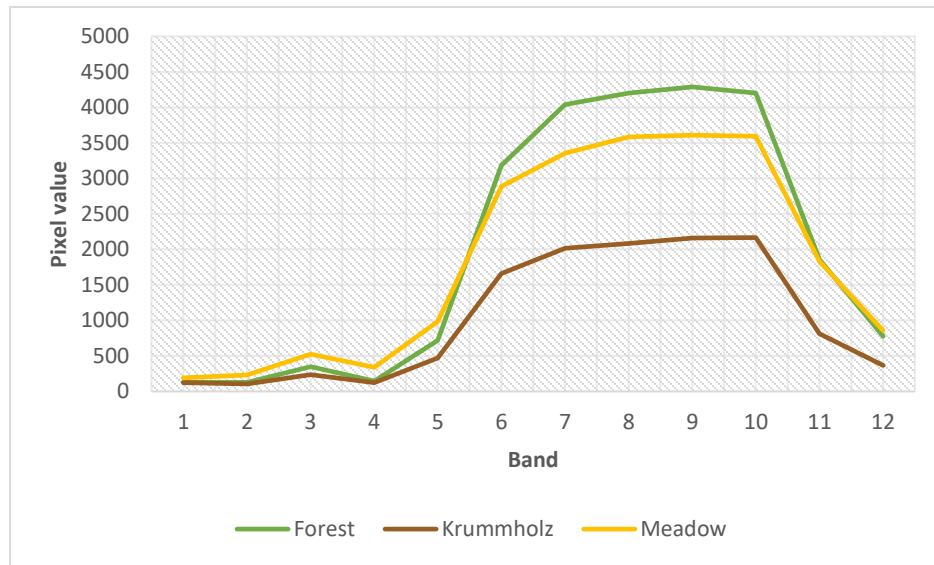
As shown in Figure 8 the training areas were chosen to allow an even distribution across the entire study area. The central region of the map (Ushba) is devoid of training areas because it is covered by glaciers and areas of rock and therefore not of interest to this study which focusses only on the natural vegetation coverage. In total 22 training areas were chosen for forest, 16 for Krummholz and 18 for homogenous meadow areas. Training areas were at least 20x20 pixels in size to allow for accurate calculations of mean NDVI for that vegetation type and subsequently the most accurate spectral signatures for classification. The average area size and description of samples taken is shown in Table 3.

VEGETATION TYPE	TYPE	AREA (METRES)	NO. OF OBJECTS
MIXED HIGH FOREST STANDS	CONIFER DECIDUOUS	5406	22
KRUMMHOLZ	CONIFER	3929.6	16
ALPINE MEADOW	GRASSES FORBS	4420.8	18

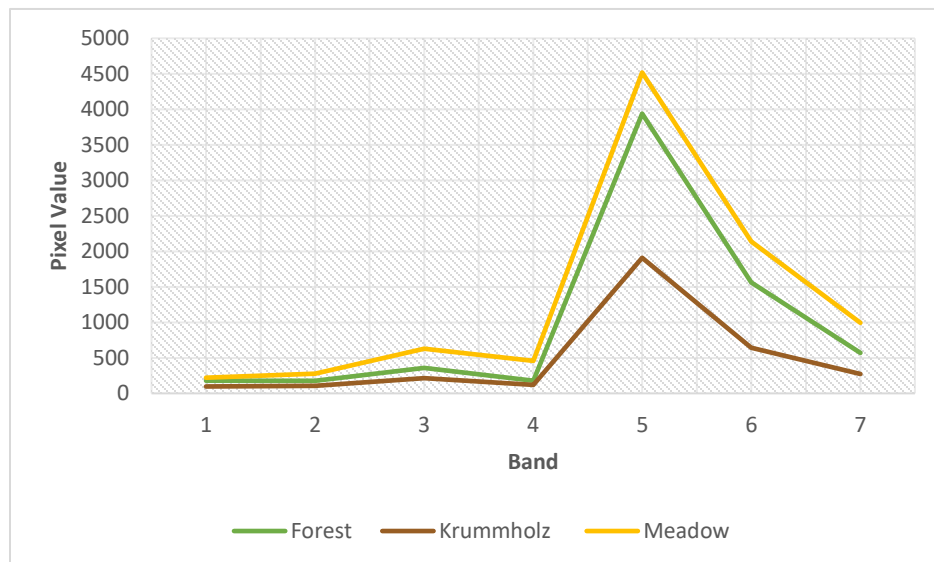
Table 3 - Description of training areas.

The mean spectral reflectance of the 3 target vegetation classes for the Sentinel-2 and Landsat-8 images can be seen in Figure 9. These graphs show the changing spectral signatures of the 3 vegetation types from a low band wavelength to a high band wavelength from left to right across the graph. Several different training areas were used to calculate a mean spectral signature at each band allowing comparison between Sentinel-2 and Landsat-8 data. As shown on the graphs the lower number of bands for the landsat-8 satellite makes the spectral curve appear more pointed but the overall values are similar (NIR plateau of ~2000 for the Krummholz and green peak of ~500 for the meadow). However, some differences are quite apparent with the meadow having a higher NIR plateau than the pine forest in the Landsat-8 images which is the opposite in sentinel-2 images. As to be expected, from previous studies such as Govender et al. 2007 [47], Smith R.B. 2001 [79], the spectral signature of the grass should be higher than that of the mixed forest stand. Yet it is possible that due to the forest stands being of mixed coniferous and deciduous species the spectral signature for this class can be quite variable depending upon location. This could therefore account for this anomaly and further the agreement that Sentinel-2 and Landsat-8 images are comparable.

As clearly shown in Figure 9 the Krummholz vegetation class emits the lowest spectral signature. This is to be expected as Krummholz is almost entirely composed of coniferous tree species which give off much lower spectral values than coniferous, grass and forb species. The meadow class emits the highest green peak as grasses and forb vegetation making up this class reflect the highest amount of green light. This is due to their rapid growth during the short summer season fuelled by photosynthesis requiring the presence of a much higher chlorophyll percentage than conifer species. The characteristic spectral curve of the three vegetation classes can be used to



(a) - Sentinel-2



(b) - Landsat-8

Figure 9 - The mean spectral signatures of the target vegetation classes ((a) Sentinel-2 and (b) Landsat-8).

compare with other possible training areas and, further, to identify the presence or absence of a certain vegetation class in that part of the Ushba region.

A fully detailed description of all the sources (references) for each of the training areas used for the classifications are shown in Table 4 - 9. The photo extract and coordinate are shown along with the type of reference used (e.g. high-resolution satellite photo or geotagged photo). As is shown within the tables, where possible, a geotagged photo was used due to its higher level of accuracy. However, geotagged photos are only present within regions of interest leaving large parts of the map uncovered. To prevent this lack of coverage high resolution satellite images at scales of 20 – 10 metres were used. Due to the image sizes and clarity, the tables for each vegetation class are split into two groups.





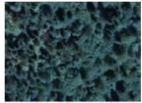

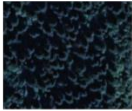




Reference Number	Image	Coordinates	Reference Used
1		43.012464, 42.591833	Google Photo Sphere Sept. 2017
2		43.022983, 42.787310	Google Satellite
3		43.040720, 42.754302	Google Shared Photo July 2020
4		43.040165, 42.732784	Google Shared Photo July 2019
5		43.040739, 42.646849	Google Satellite
6		43.026721, 42.656242	Google Satellite
7		43.045320, 42.664960	Google Satellite
8		43.012677, 42.574404	Google Satellite
9		43.052108, 42.618792	Google Satellite
10		43.071912, 42.625263	Google Satellite
11		43.079913, 42.644091	Google Shared Photo Aug. 2019

Table 4 - First half of the description of training area references for the Forest Class vegetation.


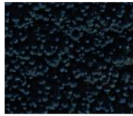
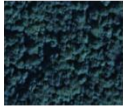




Reference Number	Image	Coordinates	Reference Used
12		43.076762, 42.612167	Google Shared Photo Sept. 2019
13		43.085997, 42.623229	Google Satellite
14		43.063659, 42.702833	Google Satellite
15		43.063440, 42.739646	Google Satellite
16		43.095068, 42.735457	Google Satellite
17		43.113681, 42.734645	Google Shared Photo Oct. 2019
18		43.051935, 42.769900	Google Shared Photo Aug. 2019
19		43.243869, 42.594812	Google Shared Photo July 2018
20		43.245159, 42.633807	Google Shared Photo Nov. 2017
21		43.228289, 42.653363	Google Shared Photo Sept. 2018
22		43.218683, 42.690405	Google Shared Photo Aug. 2020

Table 5 - Second half of the references for the Forest Class vegetation.




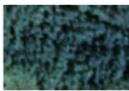






Reference Number	Image	Coordinates	Reference Used
1		43.085227, 42.527705	Google Satellite
2		43.072229, 42.540813	Google Satellite
3		43.078219, 42.576685	Google Satellite
4		43.048929, 42.645154	Google Satellite
5		43.059131, 42.659611	Google Satellite
6		43.027726, 42.724256	Google Shared Photo June 2017
7		43.021390, 42.751880	Google Shared Photo Aug. 2018
8		43.090131, 42.723153	Google Satellite
9		43.102997, 42.756154	Google Satellite
10		43.114217, 42.729077	Google Shared Photo July 2019

Table 6 - First half of references for the Krummholz vegetation class.







Reference Number	Image	Coordinates	Reference Used
11		43.127818, 42.597164	Google Shared Photo Sept. 2019
12		43.061385, 42.571511	Google Satellite
13		43.221266, 42.807503	Google Shared Photo Aug. 2019
14		43.240470, 42.784924	Google Shared Photo Nov. 2017
15		43.212736, 42.715335	Google Shared Photo Aug. 2018
16		43.210685, 42.594769	Google Shared Photo Aug. 2019

Table 7 - Second half of references for the Krummholz vegetation class.











Reference Number	Image	Coordinates	Reference Used
1		43.044462, 42.635684	Google Satellite
2		43.048507, 42.639449	Google Satellite
3		43.056994, 42.646761	Google Satellite
4		43.066267, 42.669908	Google Satellite
5		43.060455, 42.671908	Google Satellite
6		43.061047, 42.677594	Google Satellite
7		43.058276, 42.583525	Google Shared Photo May 2020
8		43.062533, 42.563719	Google Satellite
9		43.029923, 42.738635	Google Shared Photo July 2017
10		43.011660, 42.761432	Google Shared Photo Jan. 2020

Table 8 - First half of references for the Meadow vegetation class.









Reference Number	Image	Coordinates	Reference Used
11		43.054795, 42.777810	Google Shared Photo July 2019
12		43.084897, 42.784899	Google Satellite
13		43.086896, 42.705317	Google Shared Photo July 2020
14		43.089211, 42.701695	Google Shared Photo Aug. 2020
15		43.240305, 42.517712	Google Shared Photo Sept. 2020
16		43.196373, 42.594974	Google Satellite
17		43.301565, 42.772569	Google Shared Photo Sept. 2020
18		43.062533, 42.563719	Google Shared Photo Aug. 2019

Table 9 - Second half of references for the Meadow vegetation class.

3.0 Method

The method of vegetation extraction used in this study relies on three main components; image segmentation, vegetation extraction and vegetation type extraction. Image pre-processing produced clear, homogenous image objects with the same projection to allow for cross-referencing and identification of training areas. 2 levels of classification were used to first identify the vegetation, extraction and thresholding using NDVI calculations followed by identification of training areas and subsequent vegetation type extraction using a method of supervised classification. The overall workflow pipeline can be seen in Figure 11 on the page below.

The pipeline shows how operations were performed in sequential steps to allow for the best overall classification product. Pre-processing and image segmentation provide the basic steps needed to start classification resulting in the formation of clean, equal image scenes. In the level 1 classification stage the vegetation NDVI threshold analysis was performed to separate the vegetation and non-vegetation components. Finally, NDVI scenes were stacked to generate a timeline of vegetation NDVI change throughout the year (Figure 10) in level 2 classification. From this it was possible to visualize the clear vegetation zonation and to extract areas of similar NDVI. In the final stage, previously identified training areas were used in supervised classification (of these NDVI stacks) to extract the separate vegetation zones and form the final product.

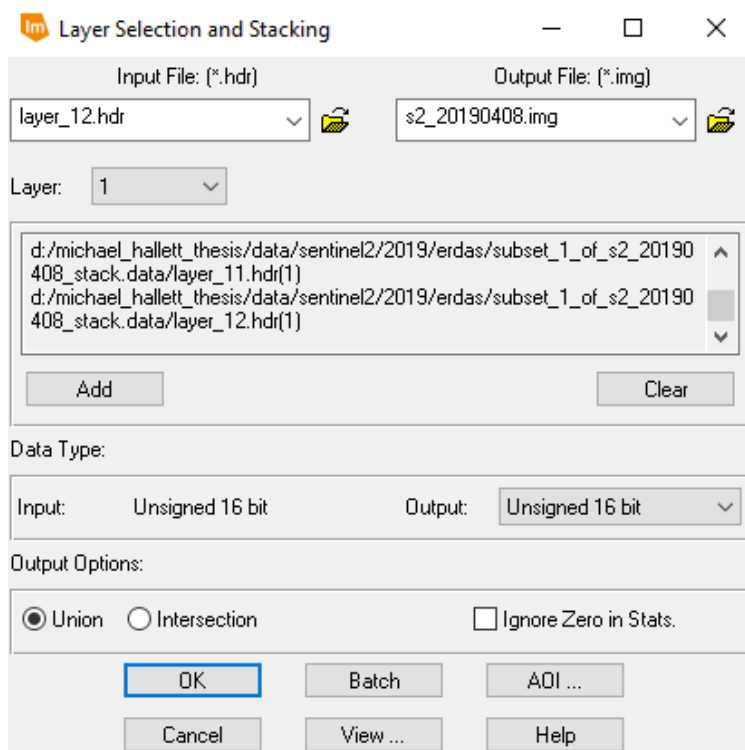


Figure 10 - Example of stacking bands using the ERDAS IMAGINE software.

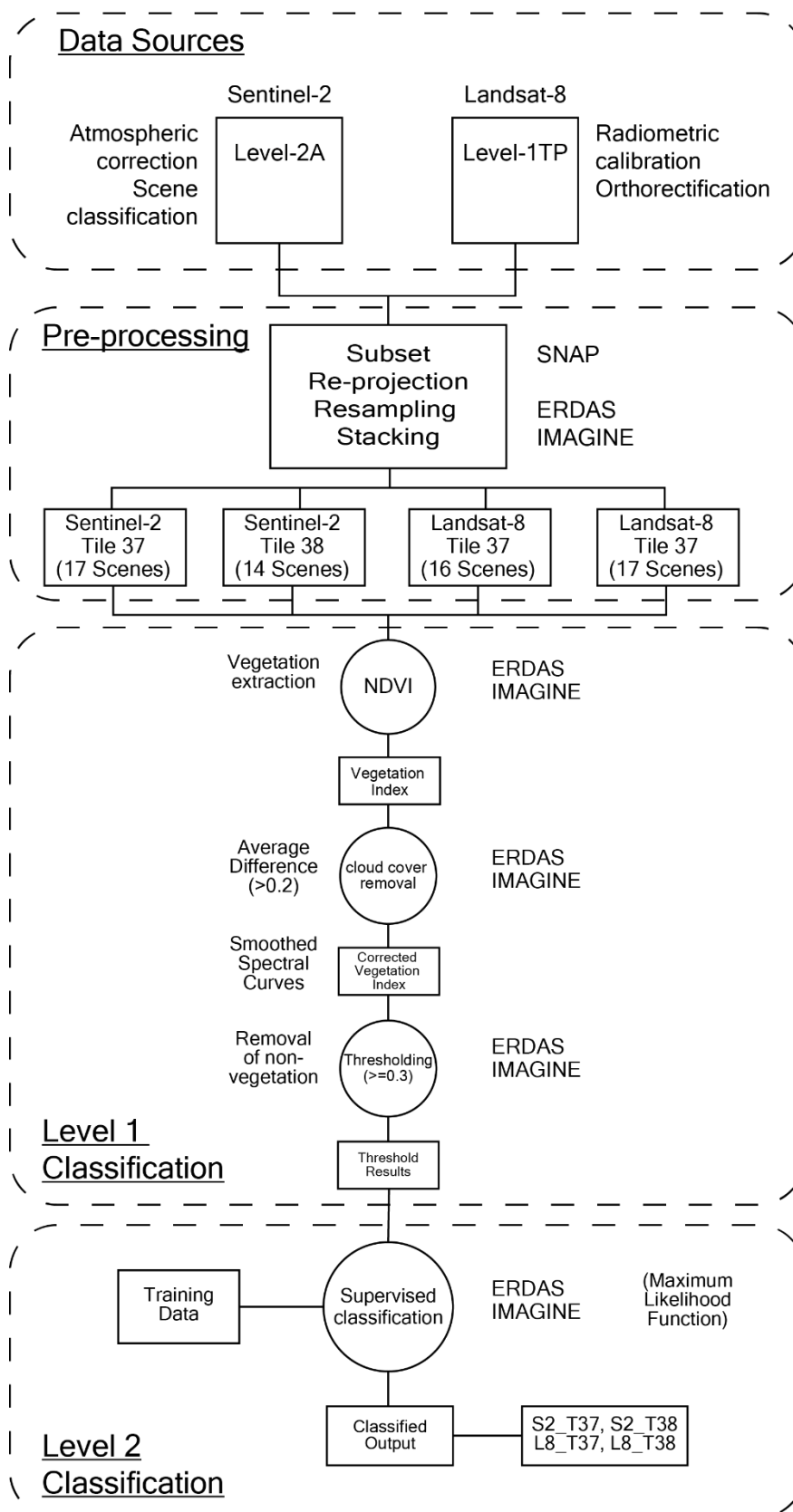


Figure 11 - Workflow pipeline of the method used in this study.

3.1 Data Pre-processing

As mentioned previously pre-processing of the data allowed for homogeneity across all data sets and produced formatted results which could then be used for the level 1 and 2 classifications. Some of the data from online data access hubs had already undergone some level of pre-processing. Sentinel level-2A products have already undergone some level of atmospheric correction and scene classification performed by algorithms. Landsat-8 products at level-1 terrain processing have undergone radiometric calibration and orthorectification using ground control points and DEM data to correct for relief displacement.

Sentinel-2 data was, firstly, unzipped and bands were stacked using ERDAS IMAGINE 2016. These stacked bands were then subset to the correct map boundary coordinates (see Figure 12) using the sentinel application platform (SNAP). This was carried out using predetermined geocoordinates that mark the boundary of the map area as agreed by members of the Ushba mapping team. Back in ERDAS the cropped band stacks were reprojected to the Universal Transverse Mercator (UTM) coordinate system and resampled to a 10m spatial resolution based on the nearest neighbour algorithm. The nearest neighbour resampling method works by assigning the digital value of the closest input pixel (in terms of coordinate location) to the corresponding output pixel in the image [80]. The advantages of using this method over bilinear interpolation or cubic convolution are that the method is simple to implement and the original pixel values are preserved. Pixel edges were also snapped so that scenes from different tiles could be overlaid during comparison (see Figure 13).

Landsat-8 data was stacked in ERDAS first before being subset to the map boundary coordinates in SNAP. The restacked bands were further reprojected to the UTM coordinate system and resampled to a 30m spatial resolution. During this phase, as with the Sentinel-2 bands, the reprojected output image stacks could be snapped at the top left corner to other reprojected image stacks to allow for easier comparison.

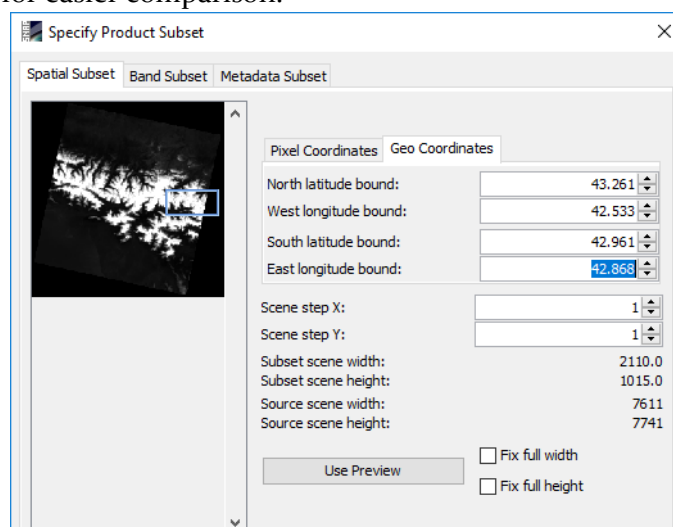


Figure 12 - Spatial subset of stacked Sentinel-2 and Landsat-8 bands to correct map boundary coordinates.

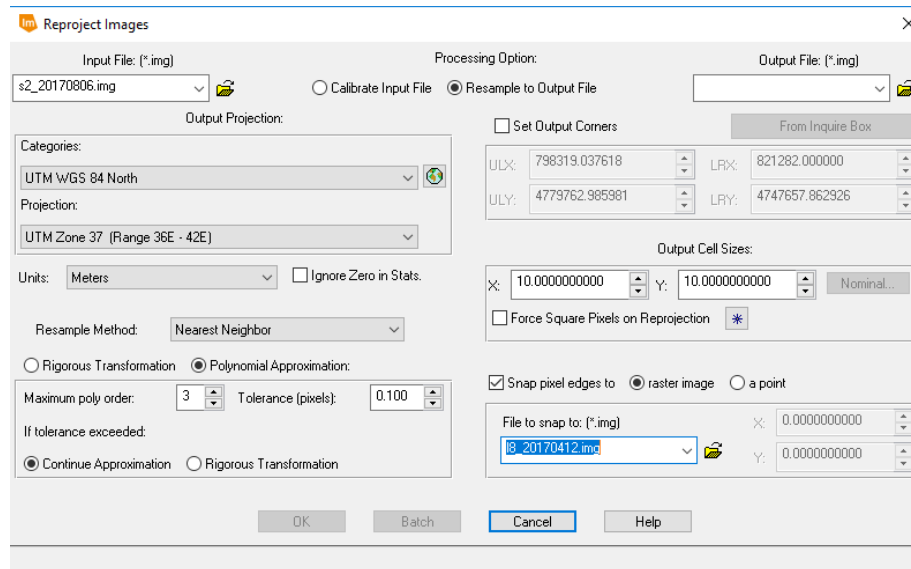


Figure 13 - Reprojection of the image stacks and resampling to correct output cell size. Output is also snapped to pixel edges of other stacks.

3.2 Level 1 Vegetation Classification and Segmentation

The first step of classification involved extracting the vegetation from the ground cover. This was carried out using the Normalised Difference Vegetation Index (NDVI) equation which is a type of threshold analysis used in numerous studies (as mentioned in the chapter 1.5) to extract the vegetation index and highlight areas of vegetation cover [50], [52], [81]. The equation used can be seen in Equation 3.

$$\text{NDVI} = \frac{\text{NIR} - \text{RED}}{\text{NIR} + \text{RED}}$$

Equation 3 - Normalised Difference Vegetation Index equation.

In this study the near-infrared and red bands were extracted automatically using the unsupervised NDVI option within the ERDAS software. It was also possible to calculate the NDVI manually within SNAP but due to the large number of scenes it was decided that ERDAS was the best and quickest method for this process. The NDVI is calculated on ERDAS by extracting the known bands which are preregistered within its software (bands 4 and 8 for Sentinel-2 and bands 4 and 5 for Landsat-8). Each sensor type is already recognised by the software from the number of bands and their wavelengths of each input image file. It's possible to select the bands for classification manually but generally these are recognised automatically once the correct category (vegetation)

and index (NDVI) are selected. It is also possible to focus on different natural elements such as certain rock minerals etc. but for this study the obvious focus was on vegetation extraction. Other indices available included the Modified Soil Adjusted Vegetation Index (MSAVI), Green Normalised Difference Vegetation Index (GNDVI) and the Ratio Vegetation Index (RVI) but these were not considered as useful for vegetation extraction within the study area. The NDVI was calculated for each scene on each individual date giving 64 products in total. These NDVI products were then stacked within their respective tiles (T37/T38) in order of dates to give chronologically ordered timelines of vegetation change throughout the growing season. From these NDVI stacks it was possible to extract the spectral signature which showed the characteristic bell-shaped curve as vegetation grows throughout the year as shown in Figure 14.

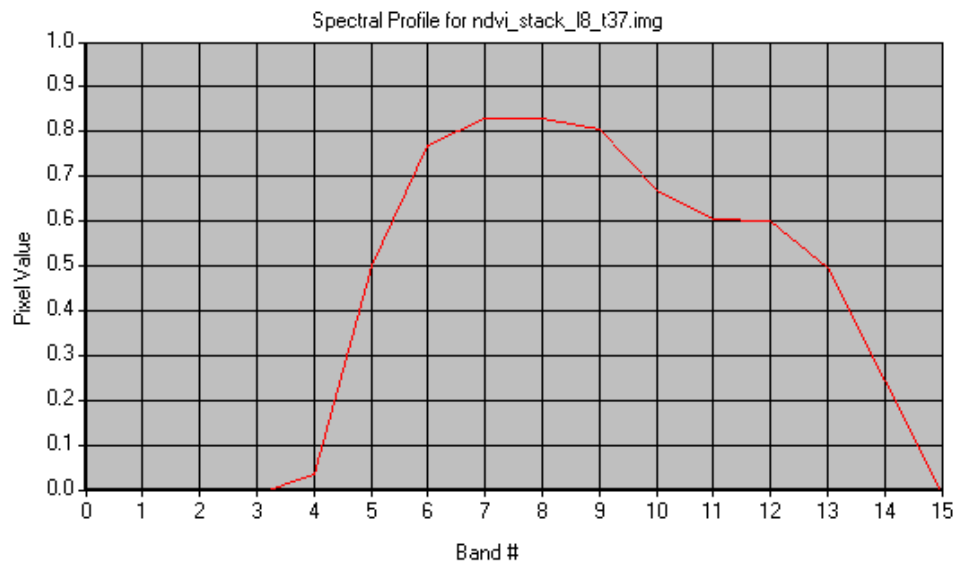


Figure 14 - Spectral profile for the vegetation index of tile 37, landsat-8 scenes. The X axis shows the image scenes in chronological order from April to November.

Unfortunately, in some of the spectral profiles, discrepancies were noticed. In some bands, large drops in the vegetation index occurred which disrupted the expected bell-shaped curve. An example of such a discrepancy can be seen in Figure 15. These were realised to be a result of cloud cover in some of the scenes which, although limited in extent, had a large impact on the spectral profile as can be seen in the graph. As a result, further processing was required to remove the limited cloud cover that was present in some of the image scenes. A model was created in ERDAS to lessen the impact of this cloud cover as shown in Figure 16. This model calculates the average difference between the two scenes in the stack that are either side of a scene. A conditional EITHER / OR function is then used to assess whether the cloud cover is present by calculating the difference between the average and the actual value. If the difference is greater than 0.2 then cloud cover is assumed present and the tile's NDVI value is replaced with the average as calculated in the previous step. The result of this method was to remove the rapid drops in NDVI value seen in the spectral profile graphs (see Figure 15) and lead towards the formation of a much smoother bell-shaped curve as seen in Figure 14. This also helped to reduce and remove anomalies from the overall NDVI stack that may have been incorrectly assigned during the second phase of classification.

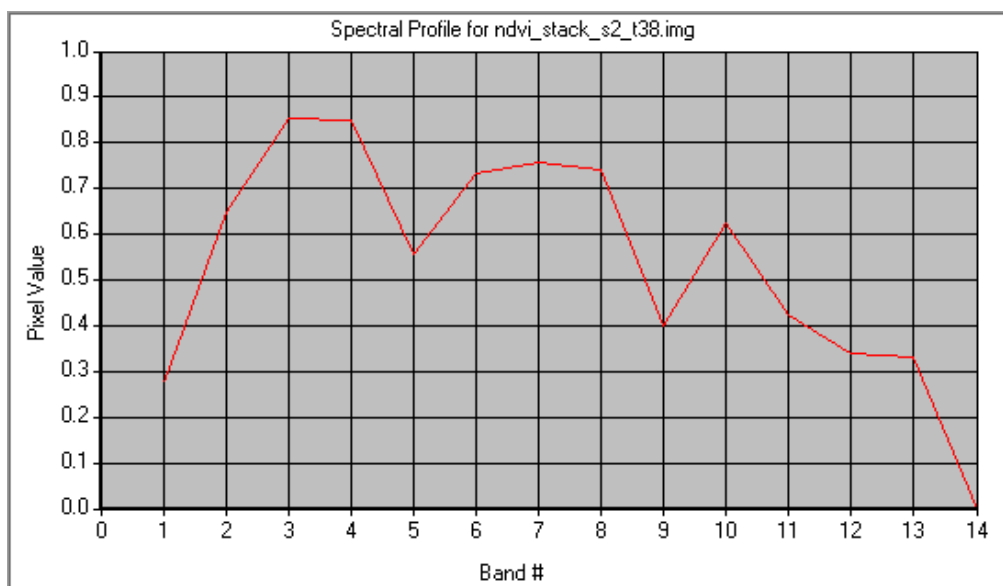


Figure 15 - Example of problematic spectral profile with probable cloud cover appearing in scenes 5 and 9.

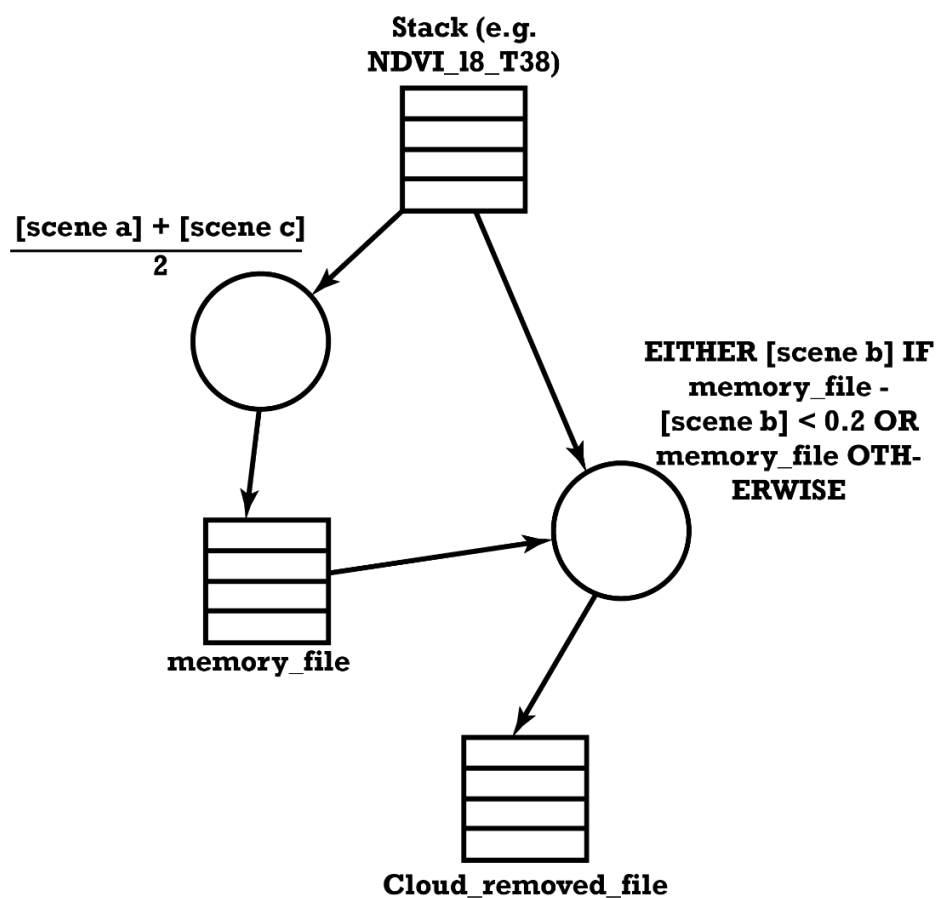


Figure 16 - Model for removal of cloud cover from individual scenes within the image stack.

The final element of pre-processing required in stage 1 was the use of thresholding to remove the non-vegetation components from the images. This was completed using a second model built using ERDAS as shown in Figure 17. This model used a threshold NDVI value of 0.3 as the cut-off point with all values beneath it removed from the image scenes within the NDVI stack. This removed any rock, ice or water that had been misrepresented as vegetation during the earlier NDVI classification. As a result of this thresholding only pure vegetation remained within the images in readiness for level 2 classification.

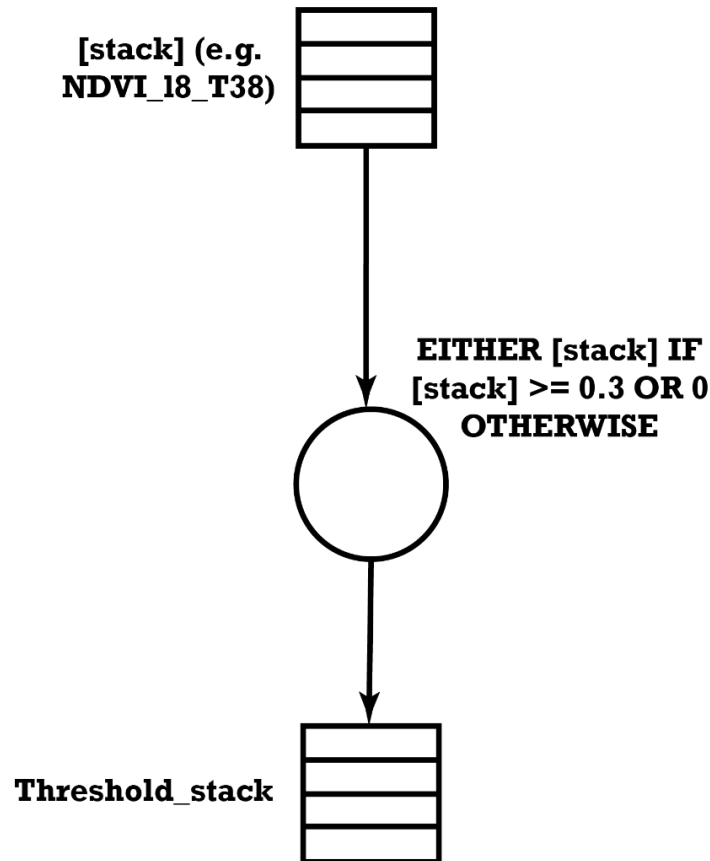
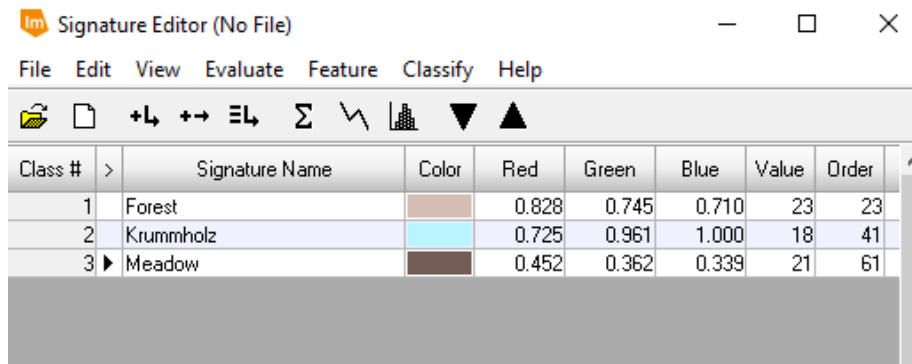


Figure 17 - Model used to add a threshold to the image scenes removing all non-vegetation from all the images.

3.3 Level 2 Vegetation Classification

The final phase of classification was to extract the individual vegetation types from the image. Supervised classification was used for this phase with the Maximum Likelihood (ML) function employed to assess whether a pixel belonged to the target class or not. The training areas, previously mentioned in part 2.2, were used for all four image scene stacks; Landsat-8 (tile 37 and tile 38) and Sentinel-2 (tile 37 and tile 38), that had undergone the pre-processing and classification mentioned earlier within this chapter. The training areas were digitised and placed within an AOI (area of interest) layer used to create a spectral signature file within the signature

editor. The signature editor is used to calculate the mean spectral values for each class and produces the spectral signature references which are used to assign a pixel to one of the three set classes. An example of a spectral signature file used in this study is shown in Figure 18.



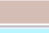


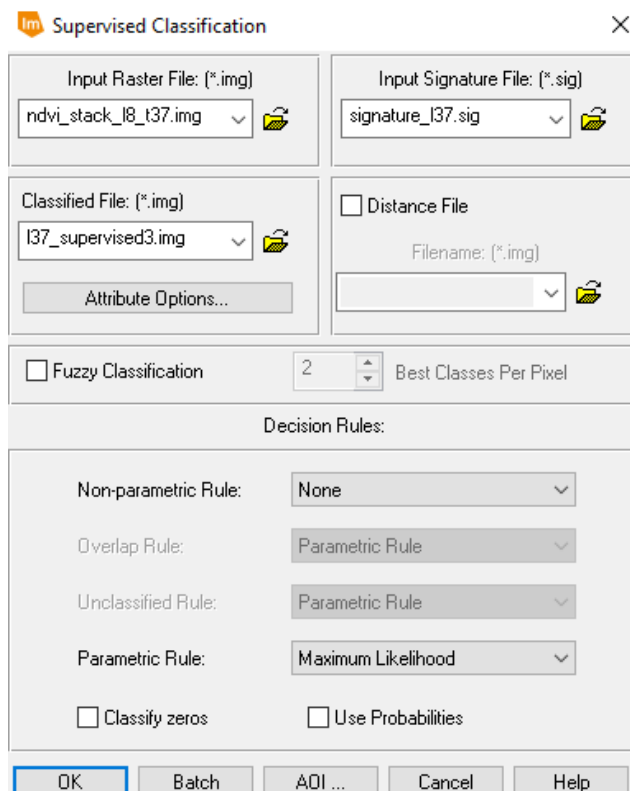
Class #	>	Signature Name	Color	Red	Green	Blue	Value	Order
1		Forest		0.828	0.745	0.710	23	23
2		Krummholz		0.725	0.961	1.000	18	41
3	▶	Meadow		0.452	0.362	0.339	21	61

Figure 18 - Signature editor for the Landsat-8, tile 37 image stack as calculated using ERDAS software.

Spectral signatures had to be calculated for each of the four image scene stacks due to the different number of scenes and bands present within each. Each spectral signature is then input into the supervised classification on the ERDAS platform as seen in Figure 19. The ML function used for this classification operation works by assuming the statistics for each class in each band



Supervised Classification

Input Raster File: (*.img)
ndvi_stack_l8_t37.img

Input Signature File: (*.sig)
signature_l37.sig

Classified File: (*.img)
l37_supervised3.img

Distance File
☐ Distance File
Filename: (*.img)

☐ Fuzzy Classification 2 Best Classes Per Pixel

Decision Rules:

Non-parametric Rule: None

Overlap Rule: Parametric Rule

Unclassified Rule: Parametric Rule

Parametric Rule: Maximum Likelihood

☐ Classify zeros ☐ Use Probabilities

OK Batch AOI ... Cancel Help

Figure 19 - Supervised classification on ERDAS using the maximum likelihood function and pre-determined signatures.

are normally distributed [82]. Each pixel is assigned to a class based on the highest probability (maximum likelihood) that the pixel belongs to that class. No threshold limit for the probability classification was needed as the threshold had already been calculated in earlier processing (see preceding section). The equation used by ERDAS is shown in Equation 4 [82]. More reasoning on the choice of ML for this study and research on the use of the classification itself can be found in the previous chapter: part 1.5.

$$g_i(x) = \ln p(\omega_i) - \frac{1}{2} \ln |\Sigma_i| - \frac{1}{2} (x - m_i)^T \Sigma_i^{-1} (x - m_i)$$

Where:

i = class

x = n -dimensional data (where n is the number of bands)

$p(\omega_i)$ = probability that class ω_i occurs in the image and is assumed the same for all classes

$|\Sigma_i|$ = determinant of the covariance matrix of the data in class ω_i

Σ_i^{-1} = its inverse matrix

m_i = mean vector

Equation 4 - Maximum likelihood equation (from the study by Richards J. 1999).

3.4 Post-Processing of Classifications

The final part of the method involved processing and extracting the classified scenes from ERDAS. Firstly, the classified files had to be recoded as each class needed to be assigned the value 0, 1 or 2 in order to be able to join different classifications together and display the classes correctly based on their attributes. Due to the way the supervised classification works each class was assigned the value, of the number of training areas used, from the spectral signature editor. For the case of the s38, used for the final classification, this was values of 25 for the forest class and 23 for the meadow class with the unclassified class remaining zero. Recoding is quite simple to implement using the ERDAS software. Within the Raster – Thematic menu the Recode function is easy to access and can be manually changed by selecting each row and inputting the new value as shown in Figure 20.

Following this stage different classification could be combined using a model in the model builder function of the ERDAS software. The different classifications could be joined in a union much like union tool on ArcGIS or QGIS. The purpose of unifying the two different classifications was due to problems with differentiating between the Forest and Krummholz classes. In most of the classifications carried out, using the method described previously, either Forest was classified under Krummholz or Krummholz was classified under Forest. However, the Krummholz classification was much larger than the Forest classification as the Forest class training sites did

Row	Old Value	New Value	Histogram	Red
17	17	17	0	
18	18	18	0	
19	19	19	0	
20	20	20	0	
21	21	21	0	
22	22	22	0	
23	23	23	3.04454e+006	0.9607
24	24	24	0	
25	25	25	2.83931e+006	
26	26	26	0	
27	27	27	0	
28	28	28	0	
29	29	29	0	

New Value: Change Selected Rows

Apply Close Help

Figure 20 - Recoding of the s38_2 classified image.

not register the actual Krummholz present in the images whereas the Krummholz class training sites did. Therefore, it was inferred that the difference between the two classification, in terms of only the Forest and Krummholz class layers, was the actual classification of Krummholz from the images. The model used to form the union was a simple model that combined the two classifications, each containing two classes, into a three-class model (see Figure 21). The resulting

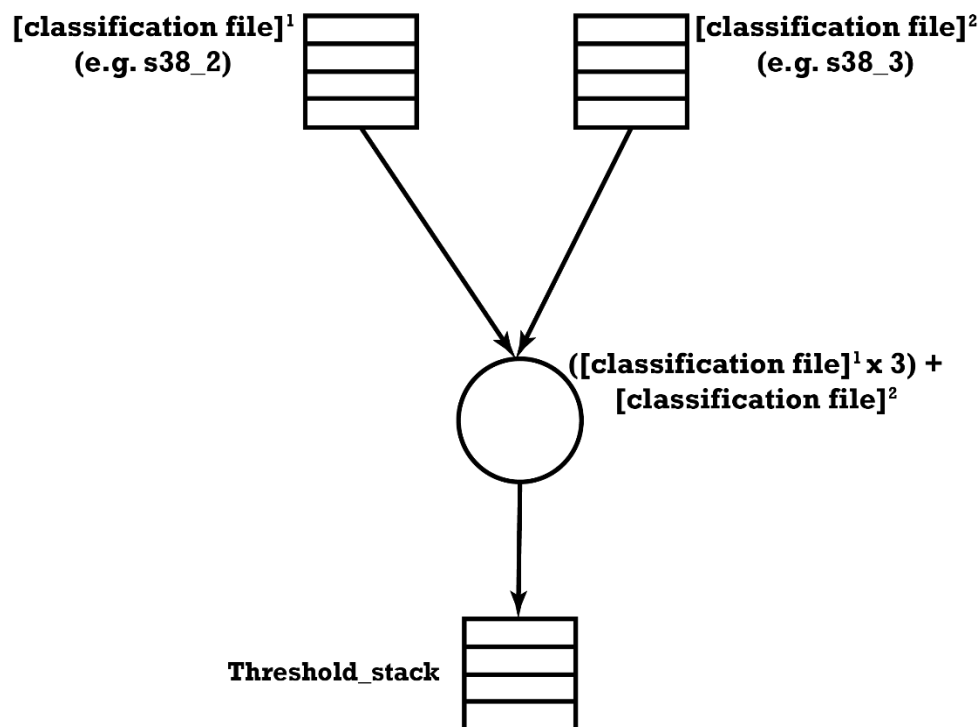


Figure 21 - Model used to unify the two classifications into a single 3-class product.

output was the final three-class output containing; Forest layer, Krummholtz layer and a combined Alpine Meadow and Herb layer.

A description of features derived from the combined pre-processing, level 1 and 2 classifications and post-processing used within the method of this study are shown in Table 10.

Table 10 - Description of the final products derived from the method used in this study.

IMAGE	FEATURE NAME	DESCRIPTION
SENTINEL-2A (31 DATA SETS)	NDVI_STACK_S2_T37 (16 SCENES)	COMBINED CHRONOLOGICALLY ORDERED NDVI SCENES FOR TILE 37 OF THE SENTINEL-2A SENSOR
	NDVI_STACK_S2_T38 (14 SCENES)	COMBINED CHRONOLOGICALLY ORDERED NDVI SCENES FOR TILE 38 OF THE SENTINEL-2A SENSOR
	S37_T	CLASSIFICATION PRODUCT OF THE TILE 37 SCENES FOR THE SENTINEL-2A SENSOR
	S38_2	CLASSIFICATION PRODUCT OF THE TILE 38 SCENES FOR THE SENTINEL-2A SENSOR (FOREST AND MEADOW)
	S38_3	CLASSIFICATION PRODUCT OF THE TILE 37 SCENES FOR THE SENTINEL-2A SENSOR (KRUMMHOLTZ AND MEADOW)
	S38_2C3	COMBINED CLASSIFICATIONS OF S38_2 AND S38_3 TO ARRIVE AT CLASSIFICATION WITH 3 CLASSES: FOREST, KRUMMHOLTZ AND MEADOW
LANDSAT-8 (33 DATA SETS)	NDVI_STACK_L8_T37 (15 SCENES)	COMBINED CHRONOLOGICALLY ORDERED NDVI SCENES FOR TILE 37 OF THE LANDSAT-8 SENSOR
	NDVI_STACK_L8_T38 (17 SCENES)	COMBINED CHRONOLOGICALLY ORDERED NDVI SCENES FOR TILE 38 OF THE LANDSAT-8 SENSOR
	L37_T	CLASSIFICATION PRODUCT OF THE TILE 37 SCENES FOR THE LANDSAT-8 SENSOR
	L38_T	CLASSIFICATION PRODUCT OF THE TILE 38 SCENES FOR THE LANDSAT-8 SENSOR

The final stages of post-processing for the classifications involved the conversion of the raster image into a vector shapefile. This was done using the ESRI software: ArcMap. From the output 3-vegetation class product, described earlier and in Table 10, the vectorisation can be easily accomplished using the ArcToolbox capabilities. Using the conversion tool, the raster image can be converted into a polygon feature (see Figure 22) with the output requirements set. In the case of this study the 'simplify polygons' button was left unchecked to prevent the formation of triangles structures within the output. The 'create multipart features' checkbox was ticked as the output must have the 3 different classes or else it would not be possible to differentiate between them within the generated shapefile. Finally, an XY tolerance of 1 metre was set to define the minimum condition for polygon features to be conjoined or stand-alone. The resulting shapefile was then symbolised using the layer properties tool where each vegetation class was assigned the colours suggested during previous thesis presentations. These colours were chosen based on their similarity to the colour schemes used in other Alpine Club maps and on their close resemblance to the colours of their corresponding natural vegetation zones. More will be discussed on the final product in the results and discussion section.

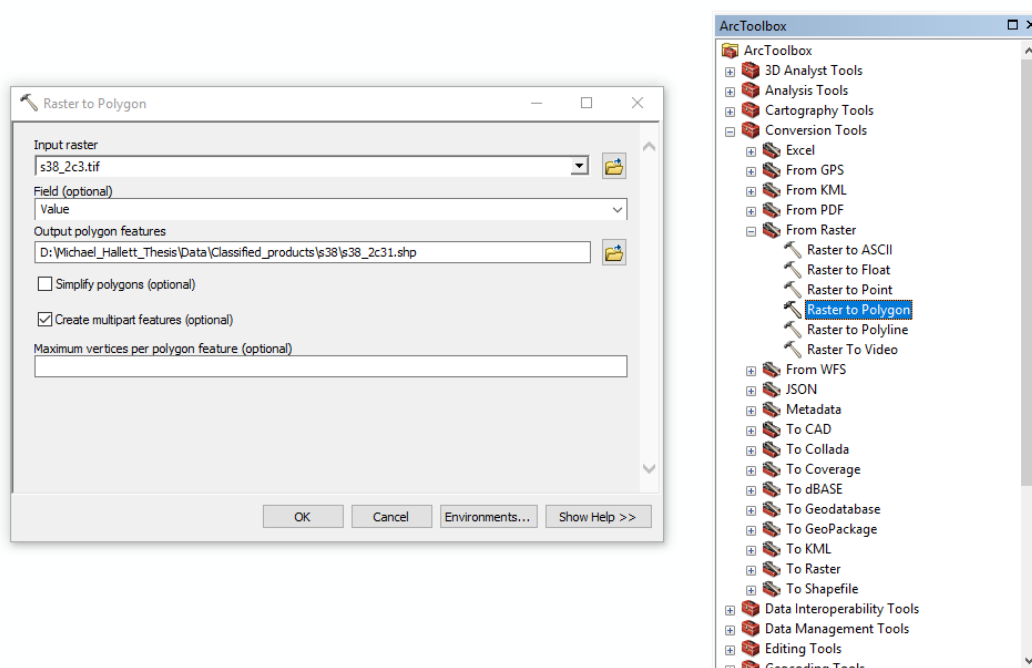


Figure 22 - Process of vectorising the raster image using tools on ArcMap.

4.0 Results and Discussion

4.1 Results of Vegetation Classifications

The vegetation classification (at the level-2 stage) was extracted within this study by use of the classic NDVI equation. Figure 23 shows the extent of vegetation cover for the area of interest with vegetation classified in green and non-vegetation classified in white. From this classification the presence of rock, ice and rivers are clearly viewed. Of interest is the presence of a large area of non-vegetation cover directly north of the town of Mestia (circled in brown). This is shown, in more detailed satellite imagery, to be the result of successive landslip and erosion which has prevented vegetation growth over this localised region. The presence of major river valleys are clearly shown with larger rivers outlined by the surrounding forest. From this image classification, the vegetation is shown as growing predominantly within the valleys something which is plainly visualised within Figure 24 and Figure 25. Figure 24 visibly shows how established vegetation species (trees and shrubs) are more dominant within the valleys where they are protected from the harsher winter snows and winds that affect the higher altitudes [2], [3]. This classification also highlights the regions of pasture and farming which exist within the valleys. These areas have been classified under the Alpine meadow layer, due to the presence of similar grassland species, and subsequently show small to medium sized, localised patches with an absence of forest. These areas, as highlighted within section 1.3, represent the high levels of hemeroby that occur throughout the Ushba region [2], [16]. Along with pastures the presence of hill tops is more noticeable within this classification as highlighted by the absence of vegetation. The most notable example of these can be seen to the south east of Mestia where a thin region showing an absence of forest runs from the WSW – ENE. This is the top of the Hatsvali ski lift and is part of a larger skiing area within the Ushba region – something which requires areas of meadow pastures with little tree cover. As noted during the introduction (section 1.0), Ushba is experiencing rapid growth in tourism and it is expected that the vegetation cover will change in the future depending upon the land use and growing need for more infrastructure [1]. Figure 25 provides an extract of mixed high stand forest which, as mentioned in section 1.3, is dominated by a mixture of tall pine and coniferous tree species. As expected from prior literature [2], [4], [15] and general knowledge of tree growth, the high forest stands dominate the lower valley sections and are particularly prevalent on the southern, more sheltered side of Ushba. On the northern slopes, and within the north facing valleys, the tree cover is sparser and more sporadic in distribution. This is to be expected as cold, northern winds likely stunt forest growth and the Ushba range itself will provide more relief for those valleys that are located to the south.

Unfortunately, due to the postponement of the field excursion, which was planned for July 2020, a lack of true field measurements prevents the ability to conduct a proper accuracy assessment for the classification. This means that the Kappa coefficient calculated for the data (section 4.8) is not completely reliable, as mentioned in section 1.5; the Kappa coefficient is used in numerous past studies [61], [73], [74] and is a useful definition for the overall reliability and accuracy of the data concerned. One way of working around this was considered: By overlaying the classification

scheme on the digital elevation model, contouring could be used to assess whether the classified vegetation zones lie within the correct elevations which were previously mentioned in section 1.3 [2], [4]. Figure 27 shows this test of the classification accuracy with mixed, high forest stands marked in light green, Krummholz in dark green and Alpine meadow in pale yellow.



Figure 23 - Extract of vegetation and non-vegetation components within the Ushba region. Scale of 1:115,000.

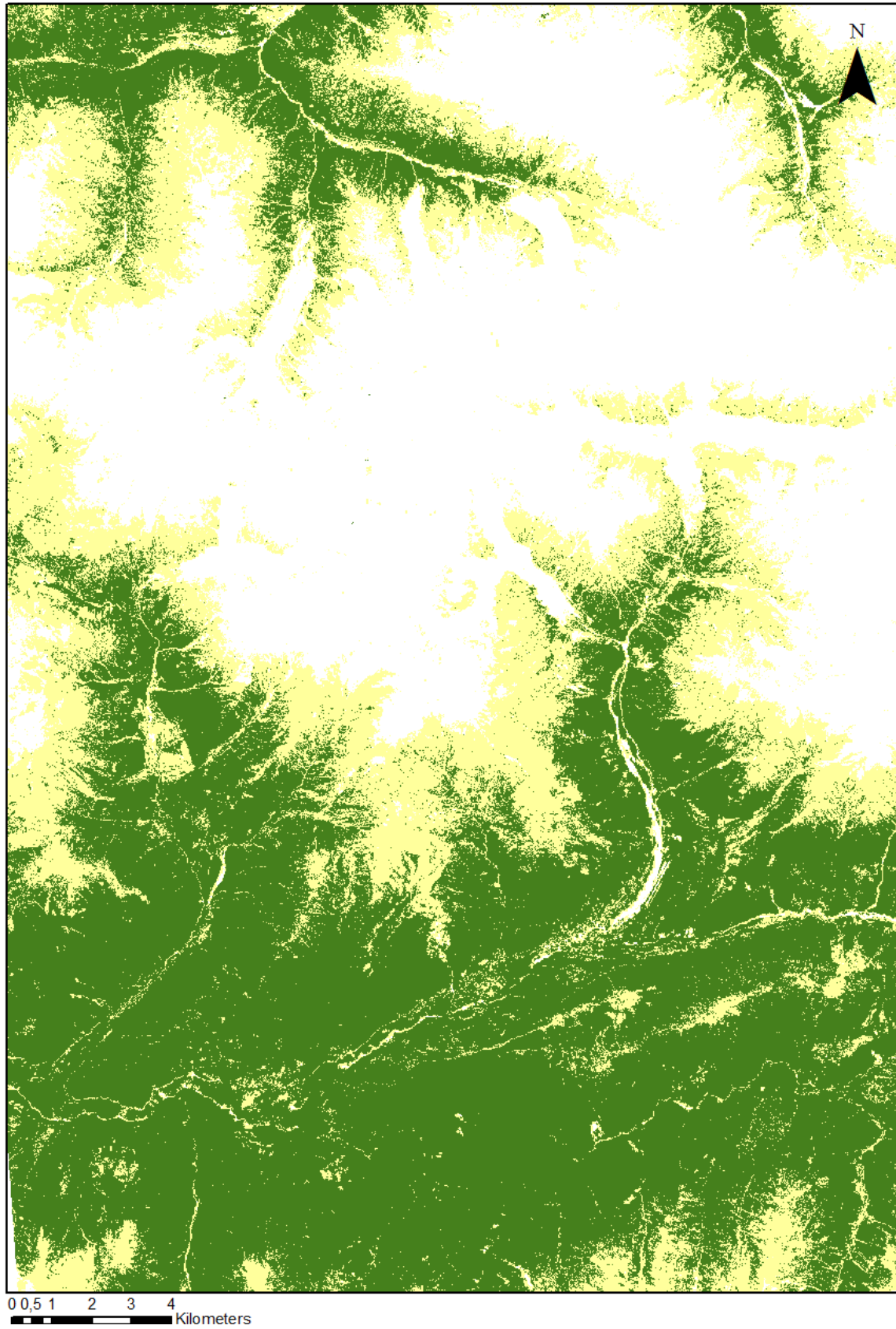


Figure 24 - Combined extract of all forest types (dark green) and Alpine meadow (light yellow). Scale of 1:115,000.

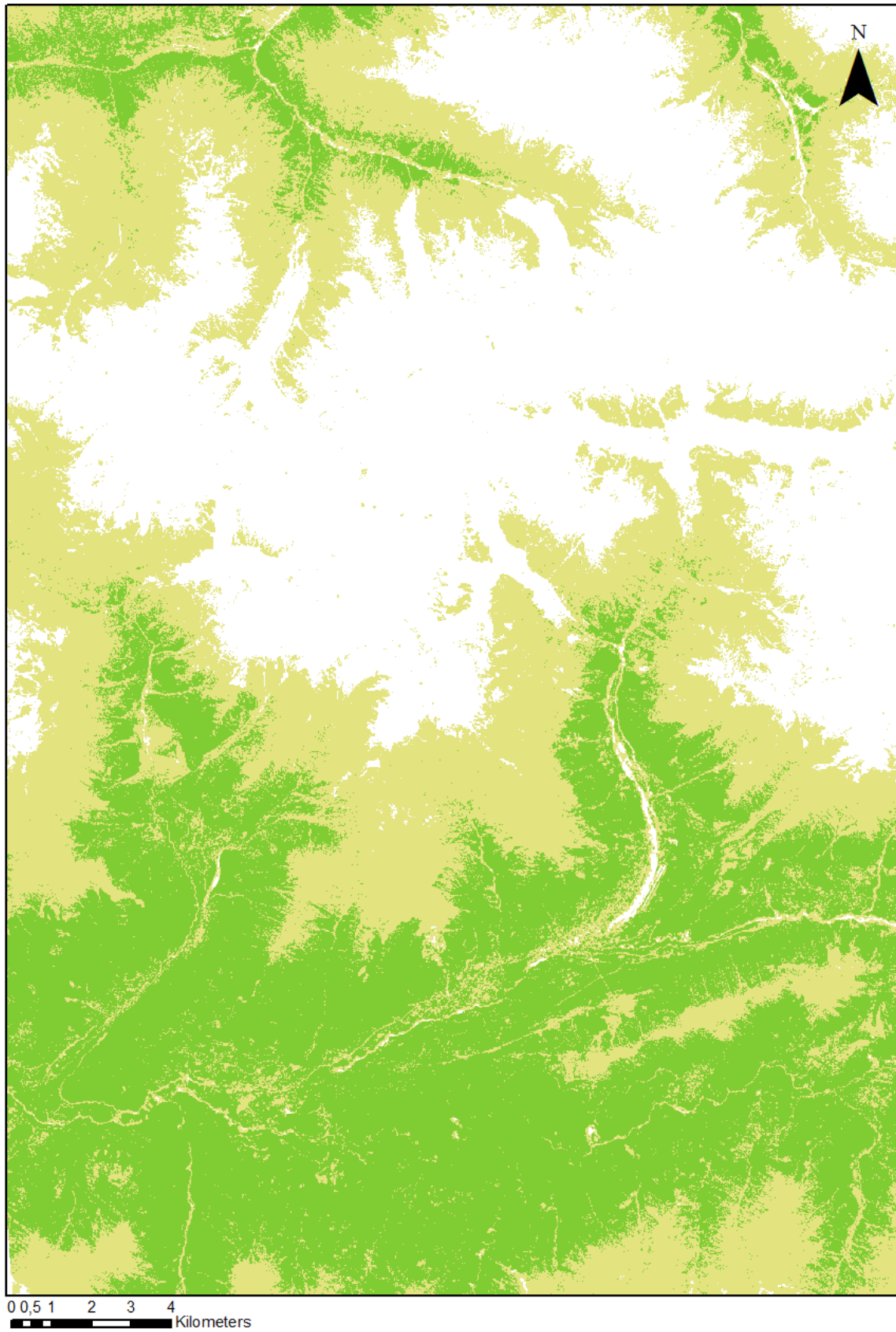


Figure 25 - Extract of only high forest stands, shown in light green, compared to other vegetation layers (Krummholz and Alpine meadow) which are shown in brown-yellow. Scale of 1:115,000.

At a height of 1500 metres, the town of Mestia, situated in the valley, is surrounded by mixed high forest stands due to its position well below the tree line. This is shown throughout Figure 27 where forest covers all the sheltered valley areas. The highest tree line observed is around 2500 metres in sheltered settings which is supported by literature in section 1.3 [2]. In Figure 26, it is possible to see an enlarged, small-scaled section of the map shown in Figure 27. Clearly shown is the existence of Krummholz between the 2300 – 2500 metre contour lines. This is again in support of detailed literature and knowledge of the usual Krummholz habitat. The maximum altitude at which Krummholz was observed is 2900 metres in sheltered valleys but this is typically within the Alpine grassland zone and is therefore rare in occurrence. Alpine grassland is shown to occur more sporadically in exposed mountain-top regions at lower altitudes (between 2100 - 2400 metres) but typically dominates at altitudes above 2400 metres. Generally, the vegetation zones, as shown in both figures, end between 2800 – 3100 metres altitude which is considered the boundary between the sub-alpine and subnival layers. As expected very little vegetation has been classified beyond this boundary due to a lack of significant vegetation cover present. Figure 26 and Figure 27 largely prove that the classification has been a success as the vegetation classes appears to exist within the pre-known altitude zones. This helps prove the overall reliability of the classification and support the classifications use for the marking vegetation on the Alpine Club map series. Figure 27 also shows the compatibility the vegetation map has with the digital elevation model and general relief of the Ushba area which further supports its use for the final map of the Ushba region.

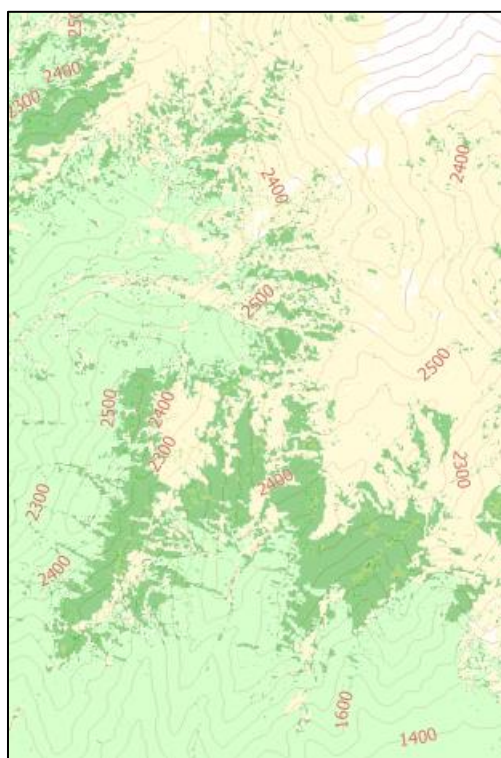


Figure 26 - Magnified view of the final classification output with contour lines marked. For the full-sized version see figure 5.

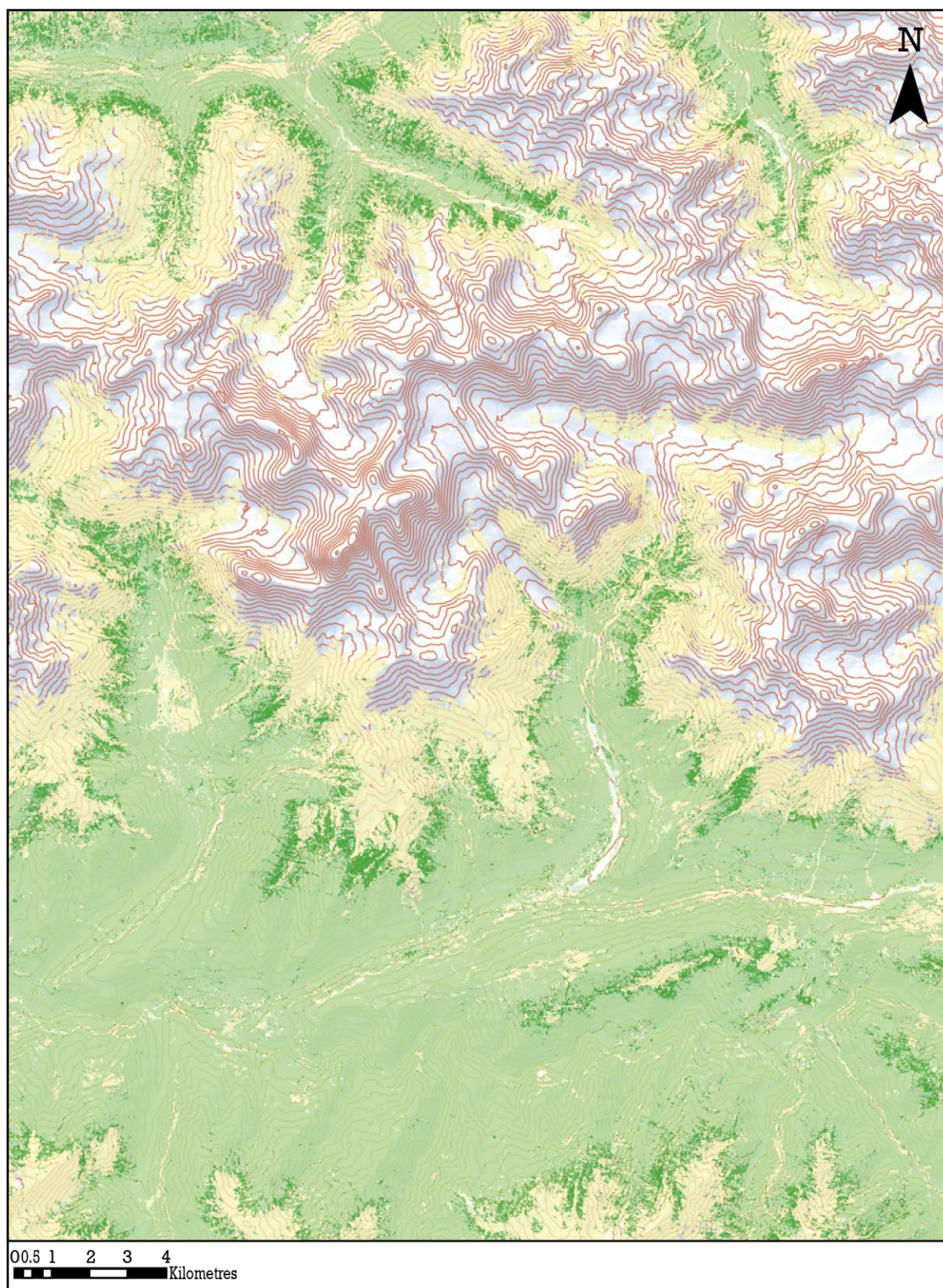


Figure 27 – Classification output (mixed high forest stands in light green, Krummholz in dark green and Alpine meadow in light yellow) overlaid on top of the Ushba DEM showing contours at 100 metre elevations. Scale of 1:115000.

The final classification output is shown in Figure 28. The colours used to represent the classified vegetation classes were chosen to allow for clear distinction between each vegetation zone. This was achieved, whilst keeping the colour scheme principally neutral, so as not to detract attention away from other map components. The colour scheme was also chosen with consideration of previous Alpine Club maps where different shades of green are used to represent the differences between the forest and Krummholz zones. The classification shows the clear zonation between mixed, high forest stands, Krummholz and Alpine meadow as a result of changes in elevation. Alpine meadows dominate the higher latitudes with Krummholz existing in the more sheltered fringes at elevations where high forest stands can no longer be supported. Smaller pockets of meadow do exist within the valleys; a result of forest clearing to make way for pastures and other farming practices, gardens or parks. The overall classification result is not perfect, and several training areas were noticed as being misclassified. The overall accuracy and Kappa coefficient will be evaluated later in section 4.8.

The classification result and its appearance reflect the usefulness of using multi-source satellite data and multiple scenes from different time periods in classifying the vegetation in an area of interest. All data used was freely available online and presents an extremely useful source in carrying out remote-sensed classifications at no cost to the producer. The Maximum Likelihood function and ERDAS IMAGINE software both represent quality tools with which an accurate and reliable classification can be produced. Overall, this classification result shows that despite setbacks resulting from external factors, a classification that appears reliable both visually and statistically can be produced from the data sources and using the tools mentioned within this thesis study.

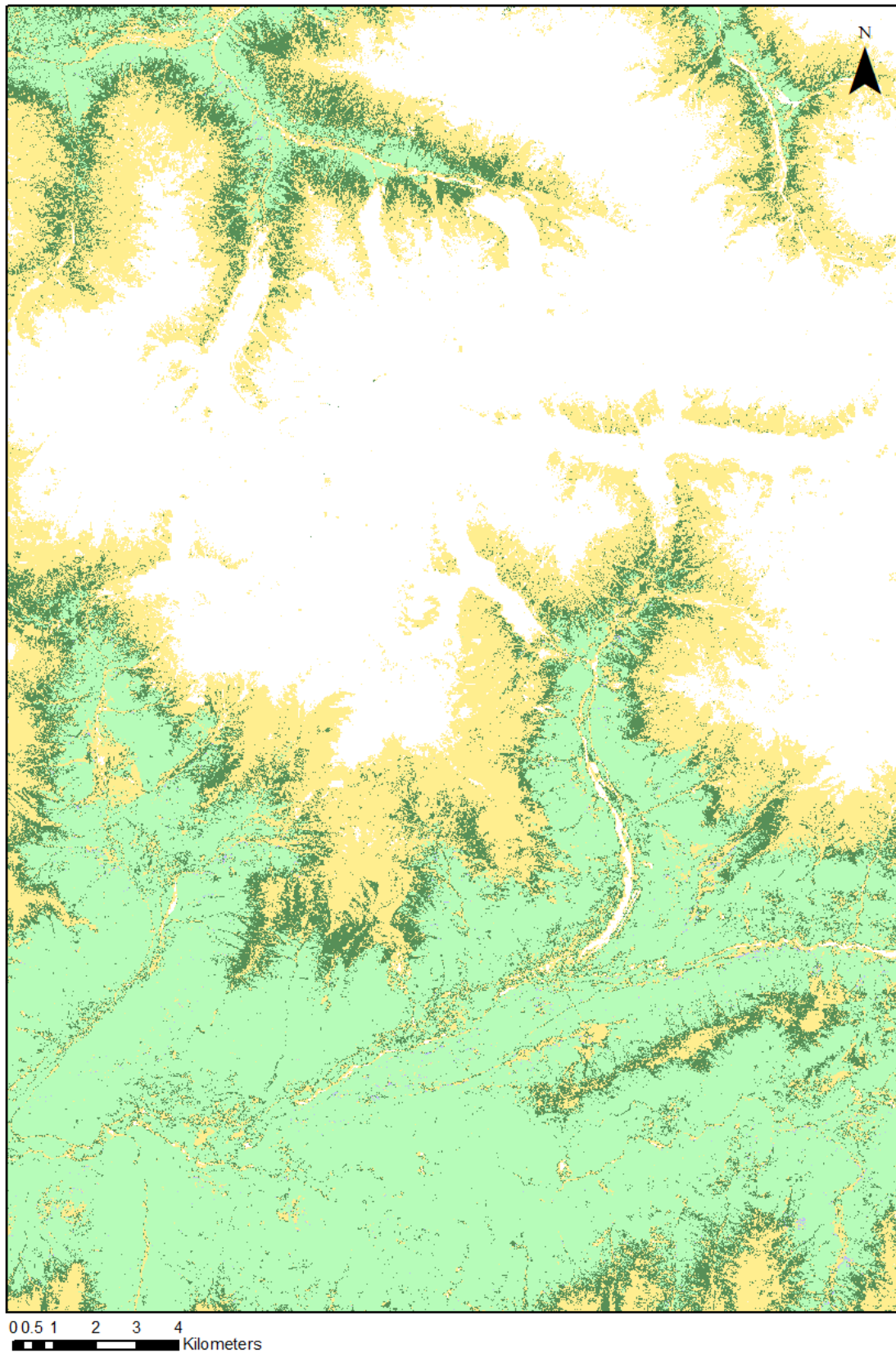


Figure 28 - Final classified product from the best Sentinel-2 scene combinations. Mixed high forest stands in light green, Krummholz in dark green and Alpine meadow in light yellow Scale of 1:115,000.

4.2 NDVI Annual Time Series

In Figure 29 and Figure 30 it is possible to view how the changes in the growing season are reflected within the NDVI classifications. As expected, the Vegetation Index increases throughout the year, reaching a peak in late August to Early September, before decreasing again into late October and November. This reflects the changing presence of green, photosynthesising leaves and their coverage on the ground. In Figure 29 (a), which reflects the start of the growing season in April, the NDVI values are mostly negative suggesting heavy snow cover over most of the Ushba region. The positive NDVI values present are mainly weak as most deciduous tree species will have not yet grown leaves and only coniferous species will be classified. This agrees with previous literature findings [47], [79], which show how coniferous species, such as pine trees, emit a lower spectral signature than coniferous species of comparable size thus accounting for the weaker NDVI signals. It is not until much later in the year (d) that the NDVI reflect the presence of these deciduous species. It can be assumed that the deciduous plant species must reach photosynthetic capabilities between May and July which agrees with the known growing patterns of species present within the Ushba region [2], [4], [20], [34]. It is also apparent from Figure 29 and Figure 30 that the snow melt occurs quite rapidly throughout April and into early May. This is reflected in the appearance of minor NDVI readings from the high mountain zone which reflect the presence of fast-growing, Alpine grasses and subnival species which grow rapidly following the snow melt [2], [4], [26]. Even until the 5th of October, Figure 30 (g), the classified Vegetation Index is quite high suggesting that leaf fall occurs after this date. This also advocates that significant snow cover must not arrive until later October or November as NDVI readings are still present, on this date, within the high mountain areas. By November (h), the NDVI is much weaker suggesting that most deciduous trees have shed their leaves and that grasses and other forb species are not photosynthesising at the same rate. Only coniferous species will still be emitting weaker NDVI signals by November as other species go into shut down in readiness for the winter months.

The NDVI time series, extracted from the Sentinel-2 satellite images, proves a useful tool in understanding the changes in vegetation cover and their subsequent timings. This is relevant to this study in furthering the understanding of how the different vegetation zones should be displayed on the map of Ushba. Different vegetation species reach peak photosynthesis at different stages throughout the year as suggested by the time series. Vegetation zones at different altitudes are affected by annual changes in temperature at different times of year which is mirrored by the NDVI value under which they are classified. This illustrates where the zonation boundaries, between forest and Krummholz and Krummholz and meadow, occur and can be used in the overall classification and mapping. One of the major issues of vegetation classification is representing the vegetation in a way that reflects zonation throughout the year. By building a time series the classification can be based; not only on a snapshot of the vegetation appearance on one date of the year, but on multiple dates throughout the entire year. This provides a more accurate classification and a better representation of the changing vegetation boundaries at different times of the growing season.



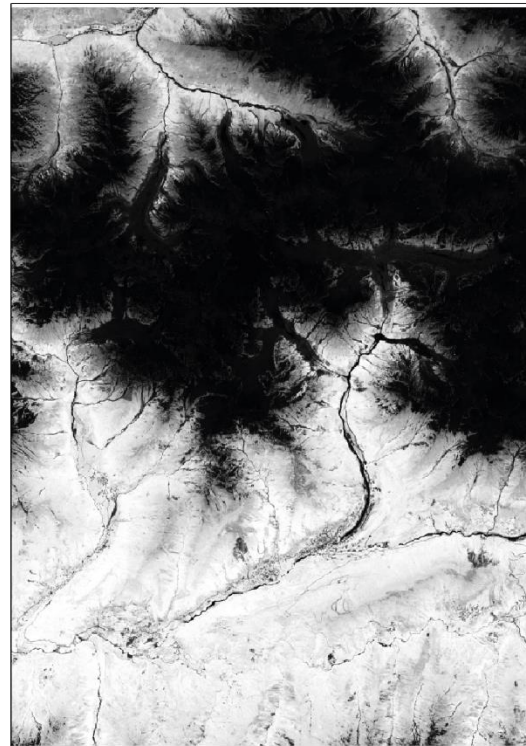
(a) 4th of April



(b) 28th of April



(c) 1st of May

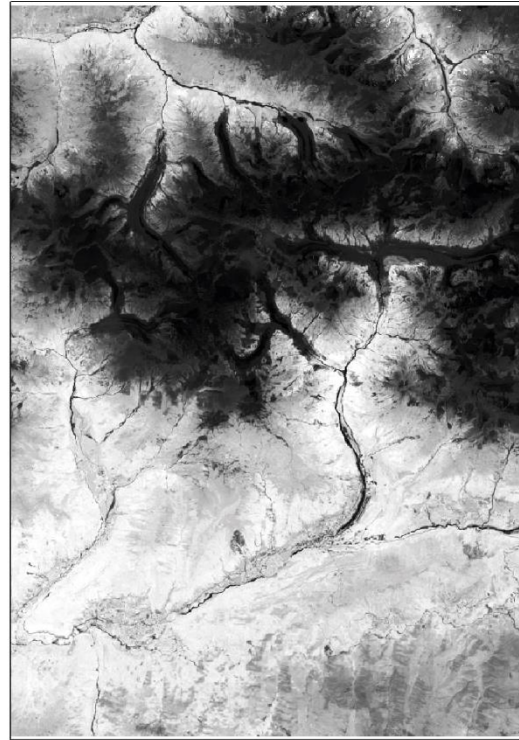


(d) 6th of July

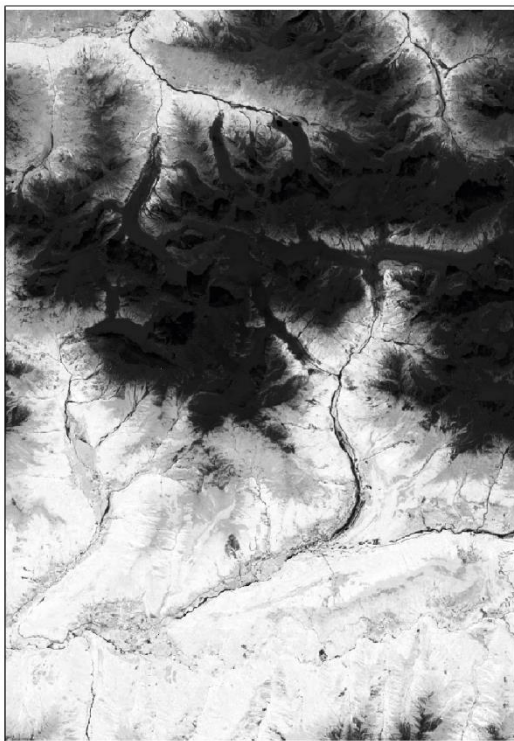
Figure 29 - NDVI times series for the Sentinel-2 satellite covering the period between April and July.



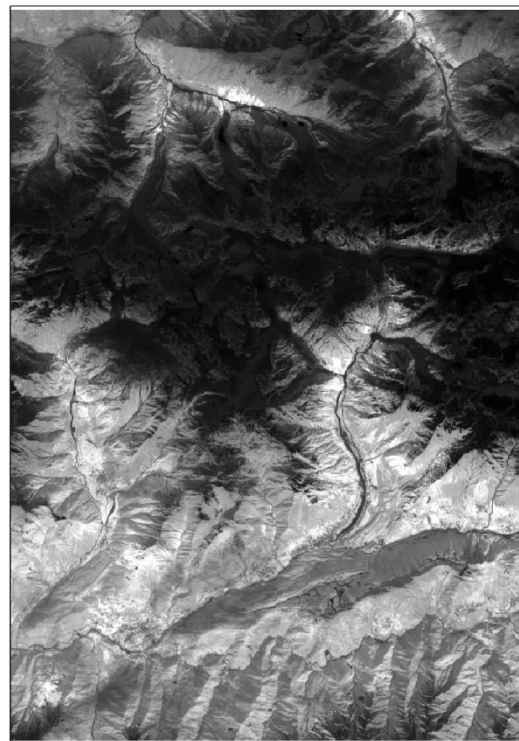
(e) 2nd of August



(f) 22nd of September



(g) 5th of October



(h) 13th of November

Figure 30 - NDVI times series for the Sentinel-2 satellite covering the period between August and November.

4.3 Yearly Comparisons

As part of this thesis study several images were taken from separate years (between 2017 – 2020) in order to give the most accurate combined classification. From each year, distinct NDVI classifications can be used to allow the comparison of different vegetation parameters between the different years. This allows the assumption and evaluation of vegetation characteristics or climatic factors for each year. Within Figure 31, this comparison is visualised with the highest NDVI values visualised in darker green and negative NDVI values in darker red. From this figure the separate years are compared across three months which correspond to three important stages of the growing season: The beginning of vegetation growth (spring), the peak of vegetation growth (summer) and the beginning of vegetation hibernation (autumn). Within the month of April, the NDVI classifications for each year appear remarkably similar. There is perhaps a slightly higher level of growth seen in 2018 suggesting warmer than average temperatures for that time of year; allowing for an earlier spring and thus an earlier growing season. This is further supported

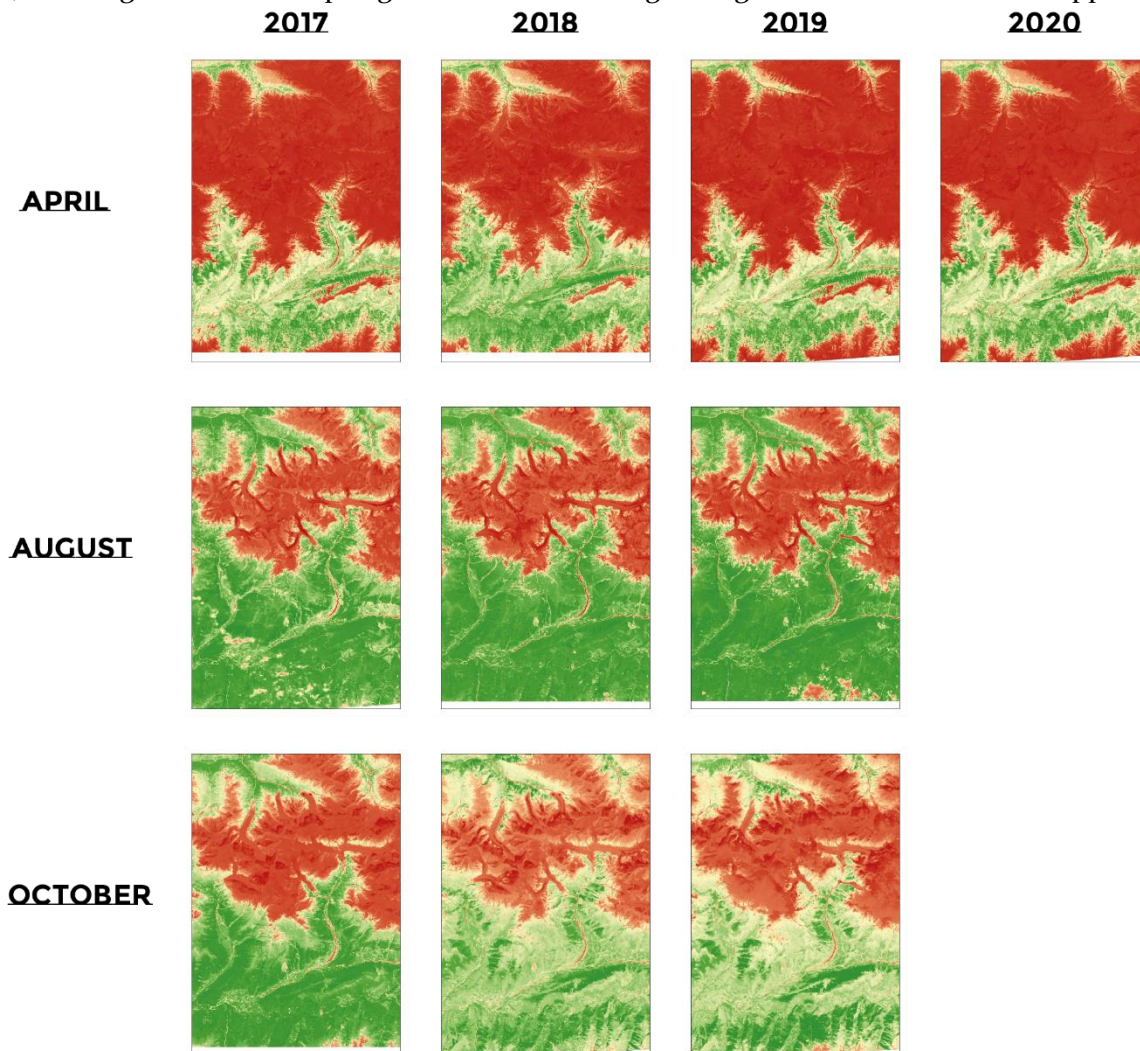


Figure 31 - Comparison between the months of different years within the Sentinel-2 image data. Images scenes were chosen based on similar sensing dates.

by the historical weather forecasts for Georgia which show the month of April in 2018 having a higher average temperature than the other years observed [83]. For the month of August, the different years again appear to display similar NDVI classification results. Slightly lower NDVI values in 2017 signify a drier or hotter summer. This is something which is again backed up by the historical weather forecasts for the region which shows a slightly less humid and much hotter August on record than other years of interest [83]. Finally, in the month of October it is very apparent that 2017 had a much later growing season than the other years. This could again be due to climatic reasons such as a later summer or more hot and humid conditions than usually experienced for October allowing for an extended vegetation growing season. However, in this case the general forecast for the region is not so supportive of this theory. Therefore, it could be due to more localised climatic factors for that year possibly influenced by the drier summer, as mentioned previously, extending the growing season later than usually seen in other years.

It is important to compare the different years as the vegetation growth changes not just annually but also over much larger time scales. By bringing together data from multiple years the overall classification is made more accurate, but it is also influenced by climate change. The well-recognised phenomenon of global warming will have a distinctive impact on the timings of vegetation growth and, in the long term, affect vegetation coverage and speciation. Within Figure 31, by comparing the different years, at selective times during the growing season, it is shown that the data used in this study is recognisably similar and can therefore be used without any worry of anomalies influencing the overall classification. In combining the image data extracted over the last three years it can be confirmed that the data is in general agreement and that any classification produced using this combination of years is sufficiently accurate.

4.4 Satellite Comparisons

Figure 32 provides a direct comparison between the Landsat-8 and Sentinel-2 NDVI classification from image scenes taken 3 days apart (22nd and 25th of September 2018). As shown in this figure, when compared, the two NDVI outputs appear virtually identical with some minor differences in the vegetation index extracted to the south of the study area. The comparison proves that although differences in spatial resolution exist, overall, the two image types are interoperable without significant processing to enhance co-ordination between the two source images. Figure 33 shows the comparison between the NDVI classified images of the two satellite types used in this study; Sentinel-2 and Landsat-8, over 3 different months. The purpose of using both satellite image types was to increase the amount of data available for the classification as well as to increase the accuracy of the overall classification by comparing between the two data sources. As mentioned in the section 2.1, the two satellites produce images of different spatial resolutions and therefore were unfit for combination. However, by creating classifications from both satellite data sets it was believed that the best overall classification could be produced from comparisons of the separate results. As seen in Figure 33, the NDVI classifications show little to no noticeable difference in resulting NDVI values meaning supervised classifications of vegetation are

comparable. The only real difference between resulting classifications is the level of detail, with Sentinel-2 results showing a slightly higher level of detail than Landsat-8 due to the differences in spatial resolution. However, at the set scale used in this study this difference is not perceptible. Resulting from this study, it is believed that although the results of classifications from the two satellite systems cannot be combined into a single classification, the use of both satellites is beneficial in achieving the best overall classification. This is possible due to allowance for a

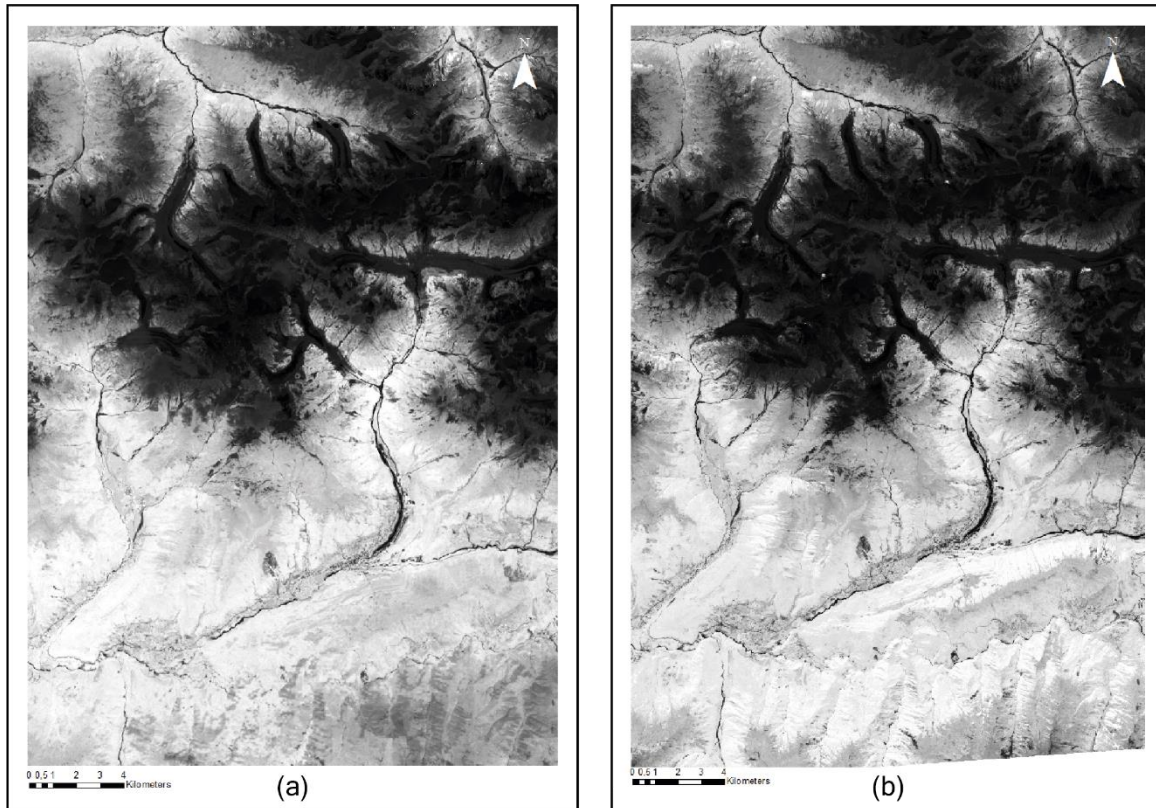


Figure 32 - Comparison between the NDVI classification taken from Landsat-8 (a) and Sentinel-2 (b). Scale of 1:115,000.

greater number of cloud-free image scenes, leading to subsequent comparison between the two results to find the most accurate vegetation classification of the vegetation within the Ushba region.

In Figure 34, the comparison between the classification results of the Sentinel-2 and Landsat-8 satellites is revealed. Despite the clear similarities in NDVI shown in Figure 33, the classification results show substantial differences between the two satellite image sources. This is despite the use of the exact same training areas as identified in chapter 2.2. The differences observed include the classification of more extensive regions of both Krummholz and Alpine meadow met with less extensive mixed, high-stand forest coverage. The differences observed are most likely due to the dates and number of image scenes used in the classifications from each satellite. With the Sentinel-2 image scenes; they are most likely formed from more peak-growing season stages of the year, whereas the Landsat-8 image scenes were perhaps originating from the beginning (spring) or end (autumn) of the growing season. This would mean Landsat-8 classifications would

not pick up deciduous trees as well as the classification using Sentinel-2 data, thus resulting in the heavier preference for Krummholz and Alpine grasses. This can be explained by differences in the strength of each classes' spectral signature with the Alpine meadow class giving the highest

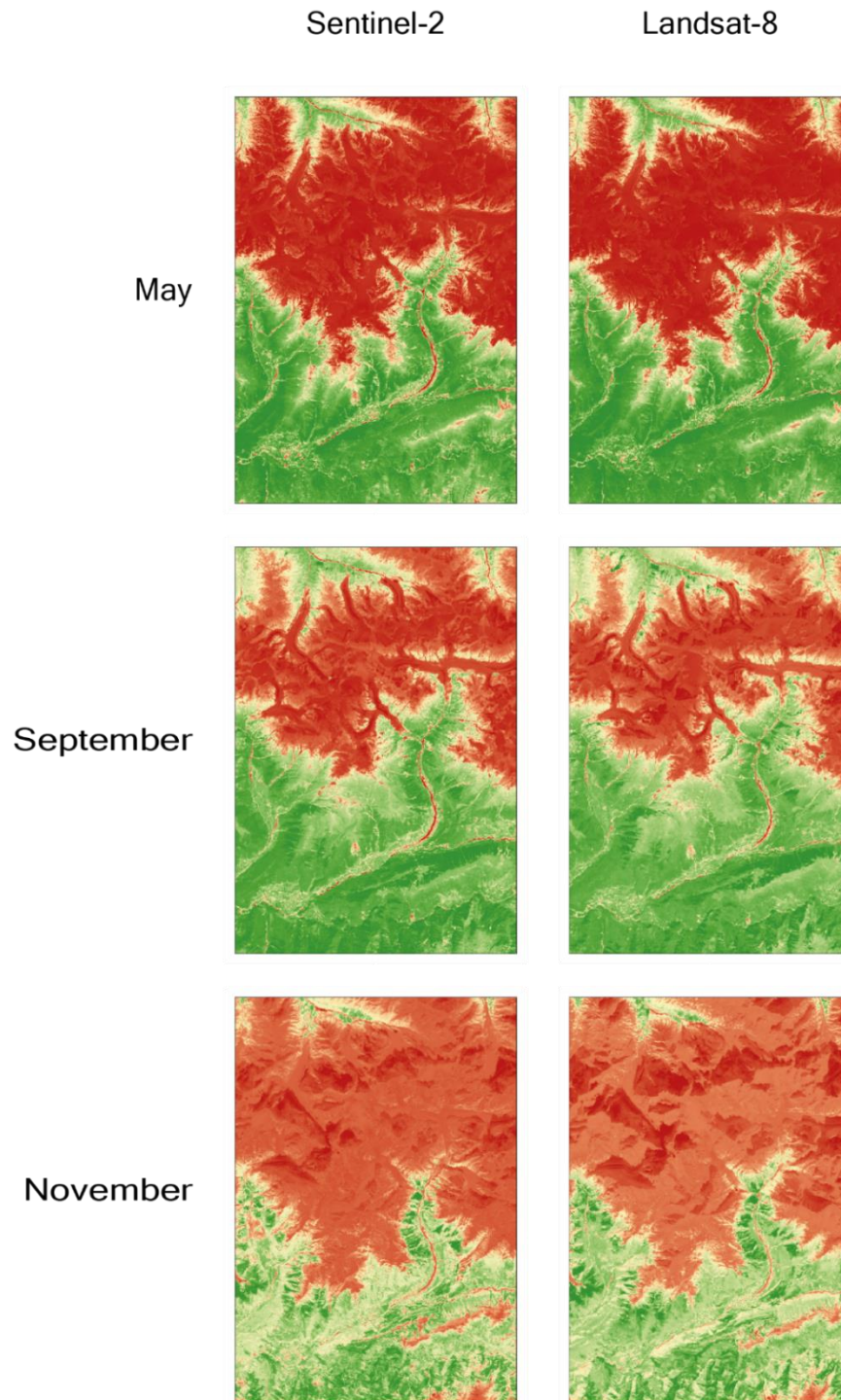


Figure 33 - Comparison between NDVI classification taken from Sentinel-2 images and Landsat-8 images over the stated months. Image scenes were chosen based on close sensing dates.

spectral signature and allowing preferent classification over the forest and Krummholz classes. Another likely reason for these variances in classification result are the differences in spatial resolution between the two satellite images. Sentinel-2 has a much higher resolution than the Landsat-8 satellite meaning classifications using Sentinel-2 data are often found to be more accurate than those using Landsat-8 images [50]. The study by Chen et al. [84], who focussed on assessing the impact spatial resolution has on classification, also supports this. They found that spatial resolution had a large effect on the spatial distribution of classification errors, and in areas of complex terrain, it was always superior to use images of a higher spatial resolution to result in the most accurate classification result. It was for the reasons discussed in this literature [50], [84], [85] and seen in the classification result, that the Sentinel-2 classification was preferentially chosen as the overall classification for vegetation in the Ushba region.

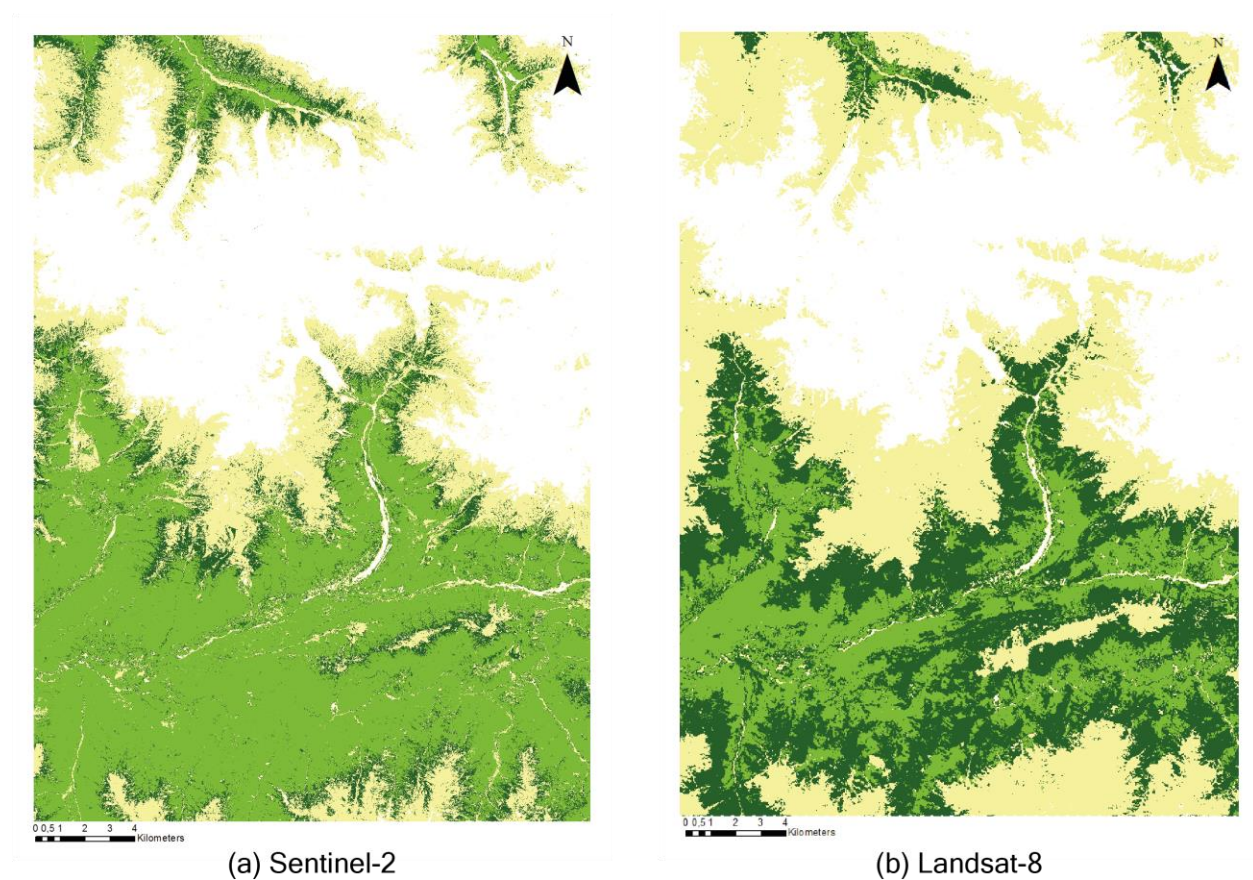


Figure 34 - Comparison between the classification results of the two satellite image types used in this study. Both at Scale of 1:115,000.

4.5 Distinction of Vegetation Boundaries

One of the primary research objectives was the question of how to represent the boundaries, between separate vegetation zones from the classification, on the final map. From looking at

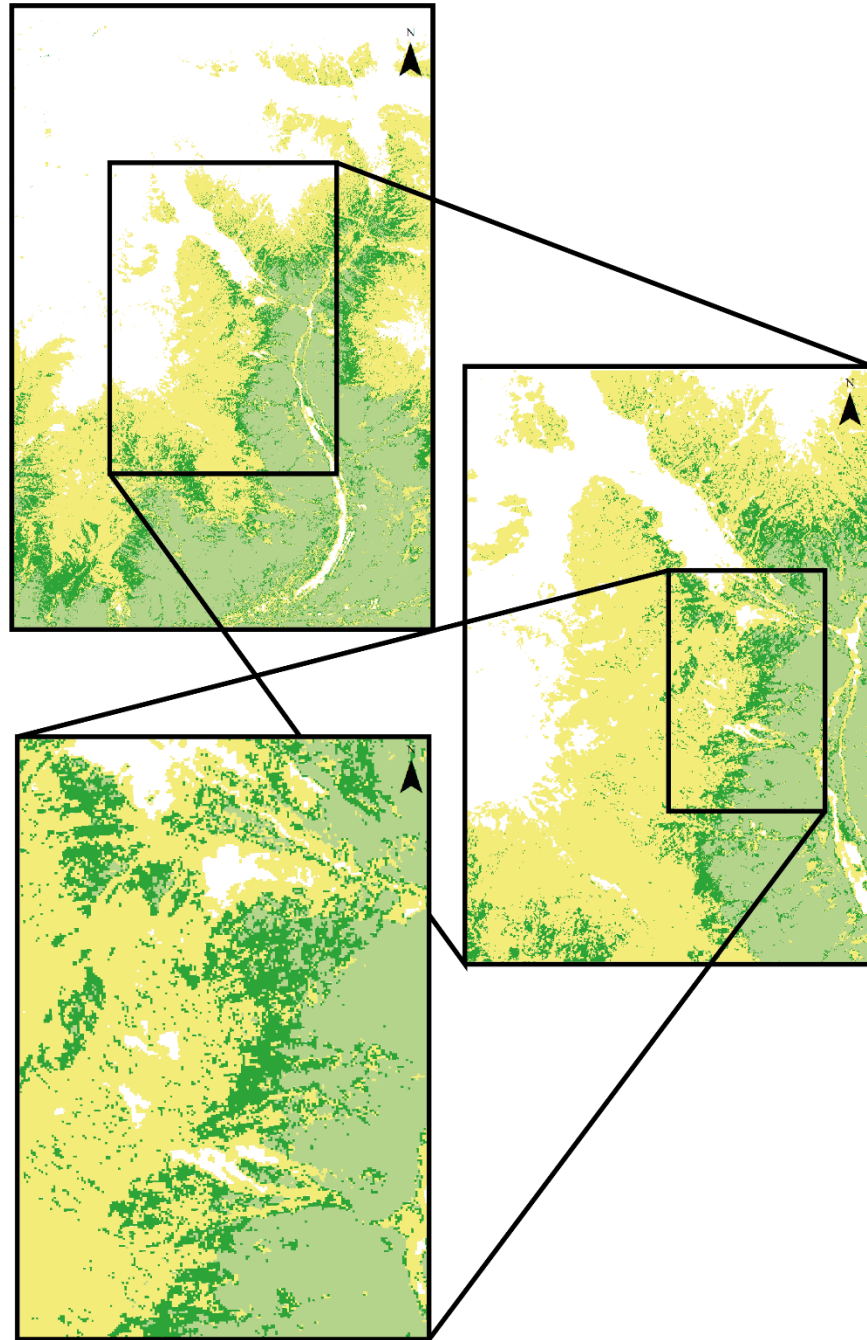


Figure 35 - Close view of the vegetation borders resulting from the classifications. Respective image scales from the top to the bottom image are 1:55,000, 1:25,000 and 1:10,000.

other Alpine Club maps and considering the classification results, it was decided that the vegetation borders would be exact and directly represent the outputs of the classification. A closer

look at the vegetation borders at different scales is shown in Figure 35. Due to the changes in vegetation cover over time, and throughout the growing season, it was considered that by representing the vegetation zones as fixed boundaries would be more helpful to the map user than representing a vague zonation border. This decision is consistent in style with the other Alpine Club maps as mentioned in section 1.4.

4.6 Timeline of Overall Classification

Figure 36 shows the timeline of vegetation classification for the Ushba region. Visualised is the growing season and class of vegetation species which dominates the visual spectrum at different points throughout the year. This figure is of interest in the case of this thesis study as it shows how classifications at different temporal snapshots can exhibit different resulting classification outputs. Shown throughout the timeline is the general increase in overall vegetation cover from April into August and September before decreasing again into October and November. This reflects the general pattern of the growing season with the peak vegetation activity and extent existing at some point in late August. This supports the discussion within the NDVI time series (section 4.2) and that shown within the yearly comparisons (section 4.3). What Figure 36 shows clearly is how each vegetation class differs in terms of peak photosynthesis. Some vegetation classes achieve peak growth (photosynthesis) earlier in the year than others as is shown in the visualisation. During the beginning and end of the growing season, Alpine meadow grassland exhibits very little photosynthetic activity meaning that classifications based on NDVI recognise very little of this class in the overall classifications during these periods. This allows for the forest and Krummholz classes to dominate classifications during the colder months as shown in April, May and November. The reason for this is the Alpine meadow species often go dormant during the winter months due to the colder climate and higher altitudes they generally occupy [2], [4]. Snow cover will also generally coexist within Alpine meadow altitudes preventing the growth of meadow species until later months when the snow has melted. Forest species on the other hand, particularly coniferous species, will not have such problems as they occupy lower parts of the valley where snow cover melts first, allowing them to spring into growth the moment snow melts and grow much later into the year than meadow species [26]. Coniferous forest species which also include Krummholz species do not have to re-grow leaves meaning they can photosynthesise throughout the year depending upon snow cover and will therefore be picked up by classifications during these winter, spring and late autumn months.

The dominance of the forest and Krummholz classes within the classification gradually ends going into the summer months. This is due to the growth of the Alpine meadow class which reaches its peak in a late August - early September time frame. Alpine grasslands dominate the classification output due to the higher spectral signature they emit (higher than mixed forest and Krummholz [47], [79]) as mentioned in section 2.2. This means that even is the extent of the Alpine grassland is small the NDVI classification of the image will highlight regions of grass over, and to the detriment of, forest areas. This accounts for the large extent of Alpine meadow cover seen from the months of August to October. The Krummholz class is shown as having its greatest

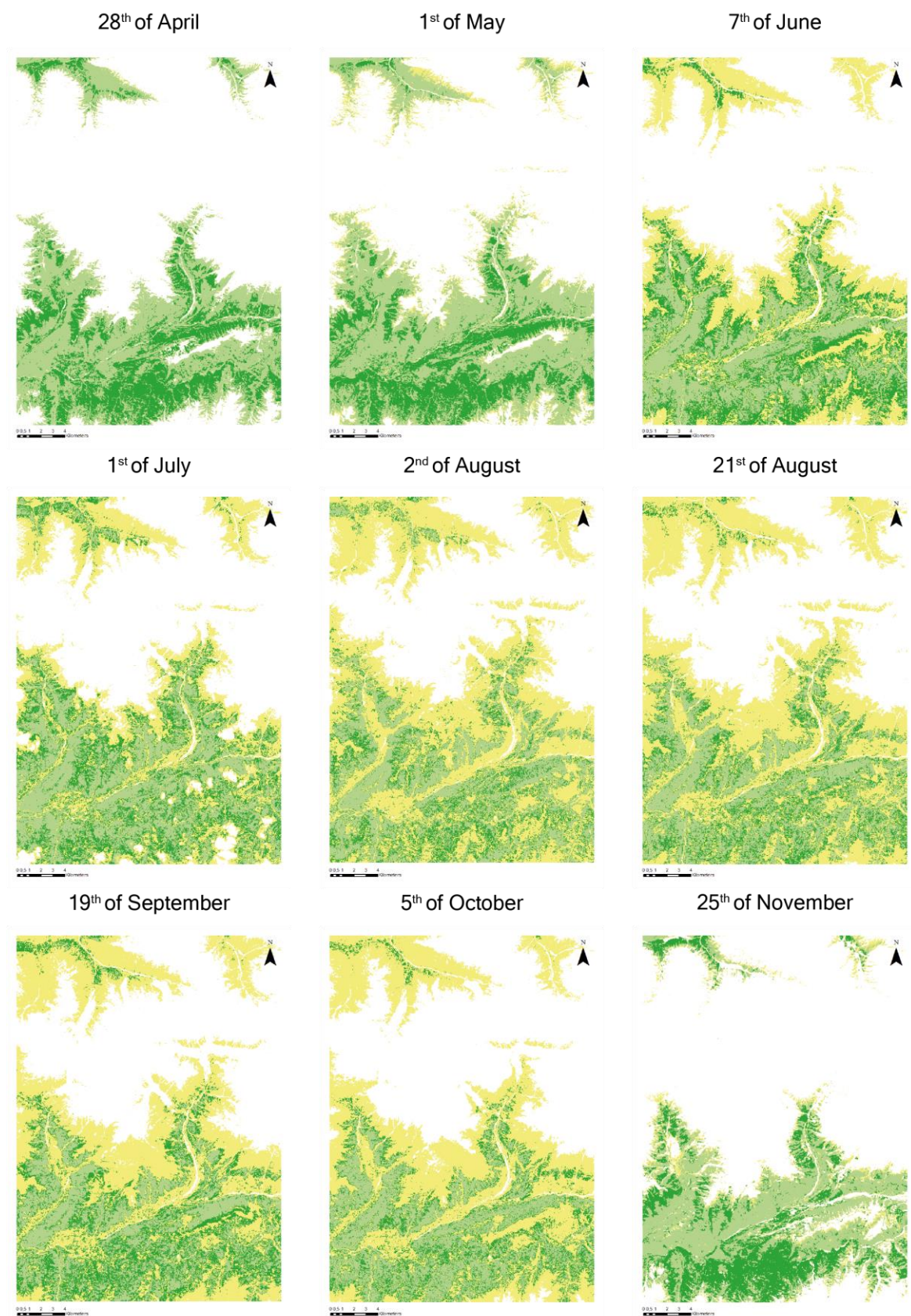


Figure 36 - Timeline of classification outputs for the Ushba region. All maps are at a scale of 1:115,000.

extent during the colder months at the start and beginning of the growing season; in April, May

and November. This is due to the type of tree species that typically constitute the Krummholz zone. As mentioned in section 1.3, Krummholz is usually made up of a mixture of crooked-stem Birch and Coniferous tree species intermixed with Caucasian Rhododendron [2]. Rhododendron is an example of a coniferous plant species which does not shed its leaves during the winter months thus allowing it to photosynthesise all year round. Birch trees are deciduous but often one of the earliest tree species to bud in spring [86], giving them an advantage over other tree species, but more importantly accounting for the dominance of this vegetation class in the off-peak growing period. This dominance of the classification output, like with that of the combined forest areas, is gradually reduced into the summer months as the deciduous tree species with higher spectral signatures reach their peak stage of growth at the end of the summer months.

Figure 36 shows the importance in the choice and combination of image scenes to use in classifying the vegetation of a region. In the context of Ushba, Forest and meadow each dominate the classification outputs during different months due to their differing annual stages of growth and spectral signatures. By combining all the NDVI classifications into a stack within this study it was possible to get the best representation of the average vegetation extent for each class at any one time of the year. Thereby the overall classification produced is the most representative and reliable output to represent the vegetation within the Ushba region. This section recognises that there is great difficulty in representing the vegetation for a specified region due to seasonal changes which can result in drastically different classifications in terms of appearance. This is something which must be considered for any study that is concerned with the mapping of vegetation using remote-sensed image data.

4.7 Forest-type Classification

In Figure 37, a classification of the separate forest types, coniferous and deciduous, is exhibited. The classification visualised here is based on training areas previously mentioned in section 2.2, as well as supplementary high-resolution satellite imagery. Sentinel-2 bands 11 and 12 (SWIR) were used to identify the difference between broad leaved and pine tree species, which is not shown through NDVI classification techniques. The same colour scheme as the final classification is used with the deciduous tree class visualised in light green, the coniferous class in dark green, and meadow in light yellow. As expected for mountainous environments, pine trees (coniferous species) dominate due to their adaptation to harsh winter temperatures and general adaptiveness to high altitude environments. Deciduous tree species flourish in the valleys where they are sheltered from high winds and protected from the harshest temperatures that exist on the exposed slopes. This is also shown in the existence of very few deciduous tree species to the north of Ushba due to the cold northern air intrusions mentioned in section 1.2 [3]. Boundaries between the two forest-type classes cannot be considered completely reliable as often areas of forest are composed of a mixture of both coniferous and deciduous tree species. In some areas of the map deciduous species are possibly over classified due to the greater strength of their spectral signature compared with that of coniferous species (as mentioned in section 2.2). However, Figure 37 does provide a rough outline of where each forest species dominates which agrees with the expected findings from previous research on the Ushba region [2], [4] and general knowledge of

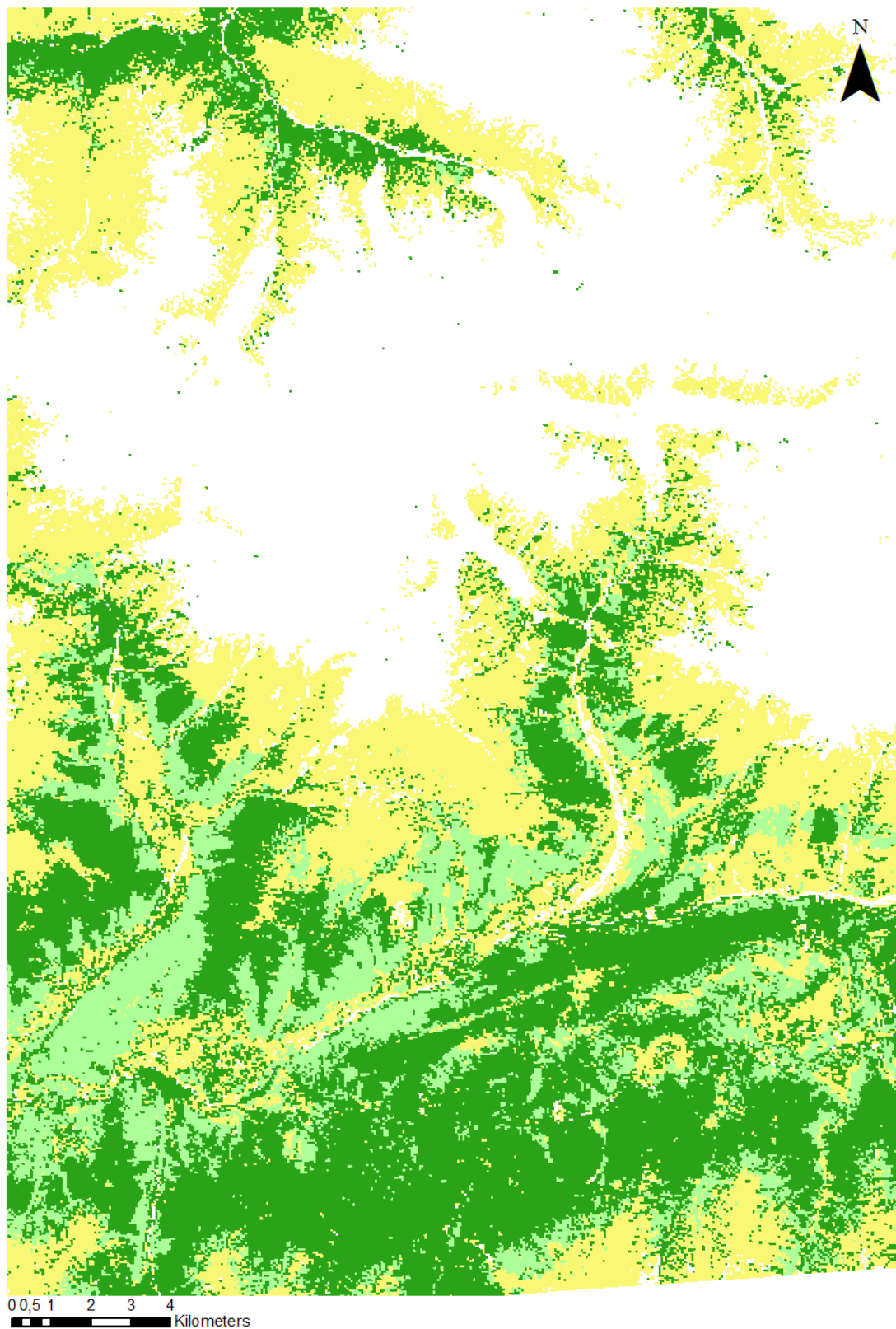


Figure 37 - Classification of the different forest types; coniferous in dark green, deciduous in light green and meadow in light yellow. Map is at the scale of 1:115,000.

mountainous forest habitats. From this classification it would be possible to add the two forest

types to the overall classification to provide more information on the regional vegetation for users of the suggested map. For the case of the Alpine Club map, it was decided not to include this information to match the general style of this map series and to prevent over-complication. As mentioned previously, due to a lack of accurate field data the reliability of this classification (along with all other classifications in this study) is questionable, but the classification closely matches the expected distribution of forest species from literature and satellite images. For future studies, the addition of reliable field data would greatly enhance both the accuracy and usability of this map.

4.8 Confusion Matrix

The confusion matrix shown in Table 11 was calculated by analysing which training areas were correctly classified and which were misclassified. The reference data is shown along the top row of the table and classifications are shown on the left side. Due to the nature and general inaccuracy of the training data sources (google photos and high-resolution satellite data) the confusion matrix cannot be considered of high reliability. Instead it can be used to show a rough accuracy assessment of the classifications carried out during this study. For the mixed, high forest stands the classification results proved mostly accurate with only two training areas misclassified as

Table 11 - Confusion matrix for the classification based on correct or incorrect classification of training areas.

	Mixed High Forest Stand	Krummholtz	Alpine Meadow	
Mixed High Forest Stand	20	1	1	22
Krummholtz	1	14	3	18
Alpine Meadow	1	1	14	16
	22	16	18	48

Krummholz and Alpine meadow. Krummholz was also correctly classified in general with again, two misclassified training areas. Alpine meadow had the lowest accuracy in classification result with 4 training areas misclassified mostly as Krummholz. This gave the Alpine meadow class a producer's accuracy of 78% calculated by dividing the number of correctly classified training areas by total number of training areas. Reasoning for this could be due to the close and often mixed occurrence of Krummholz within Alpine meadow zones leading to a higher occurrence of confusion during classification. The overall accuracy from the classification result was 86% which, despite the lack of precise field data, signals a respectable outcome. The lowest user accuracy was achieved for the Krummholz class with a value of 78% and the highest error of omission was 22% for the Alpine meadow class. Overall a Kappa Coefficient value of 0.78 was calculated for the classification output which corresponds with values from other reputable studies [50]. The Kappa Coefficient was calculated using Equation 5 shown below and is a very useful statistical tool for evaluating the quality of the classification. Despite the lack of true field data measurements, the accuracy values and Kappa coefficient show a positive classification result. Overall, the classification produced appears to match the natural presentation of vegetation in the Ushba region and the vegetation layers produces from this classification can be used to accurately describe the vegetation zones.

Equation 5 - Kappa Coefficient.

$$K = \frac{n \cdot \sum n_{ii} - \sum n_{i+} \cdot n_{+i}}{n^2 - \sum n_{i+} \cdot n_{+i}}$$

$$K = \frac{56 \cdot 48 - 1060}{56^2 - 1060}$$

5.0 Conclusions

In this study, the classification of vegetation zones around the Ushba region was carried out using freely available, remote-sensed images to arrive at a classification of three, separate vegetation classes. The resulting classification and annual time series can be used to clearly interpret the phenology of the three vegetation zones and classify the borders between them. The three vegetation zones classified; mixed, high forest stands, Krummholz and Alpine meadow, represent amalgamations of vegetation species found in distinct zones within the Ushba region as noted in literature and imagery. The choice of these classes was based on prior knowledge of other Alpine Club maps and the reliability of classifications carried out using the available data. The final vegetation-type map was generated using hierarchical classification that made use of commonly used classification practices as outlines in previous research and available to implement using the ERDAS IMAGINE software. The method provided a clear approach to achieve an accurate and reliable classification using the training data accessed from online resources which replaced the

lack of true ground data from the field. A confusion matrix calculated using the training data showed an overall accuracy of 86% and a Cohen's kappa value of 0.78. Although these values cannot be considered completely reliable, they suggest the classification is accurate. This is something which is also supported by the clear zonation showed in the final vegetation map reinforced by previously discussed literature and knowledge of vegetation zones in similar mountain ranges.

The vegetation was symbolised in a way that closely matches with other Alpine Club maps. Distinct vegetation boundaries were proposed to clearly represent where one vegetation zone finished. This is something which is often not the case naturally but provides clearer information for users of the map when navigating. The use of hard vegetation boundaries is also something which is used in present Alpine Club maps, so it was considered as fitting the general theme of this map series. Neutral colour tones were chosen to allow the vegetation to act as the map background rather than dominate the viewers' attention and so not to detract visually from more important map components. The final map layers show clear representation of the vegetation zones within the Ushba region, and therefore completes the overall aim of this study as well as answers the accompanying research objectives. Consequently, the vegetation layers are suitable for use on the suggested Alpine Club map, at the suggested scale of 1:33,000, with full-scale versions available for viewing within the digital appendix.

As mentioned in the beginning of the introduction, the Coronavirus pandemic had a large impact on the feasibility of carrying out the classification of the study area as well as on the quality of the classified results. For a more reliable classification, there is a requirement for accurate ground truth data retrieved from the Ushba region itself. The planned Ushba field trip has now been postponed until July 2021 where it is hoped that the recovery of accurate field data can be achieved. Within the studied literature, the progress of vegetation classification throughout the past 20 years has increased greatly due to developments in software and satellite imaging technologies. Although ERDAS is a reliable image processing software ENVI seems to be the preferred software due to amount of possible classification techniques which can be conducted using it. These include the use of Machine Learning Algorithms (MLAs) which produce more reliable results and can distinguish between a much higher number of classes. Despite the existence of better software and higher resolution remote-sensed images, the classification conducted in this study represents a method that used the available resources to arrive at an accurate classified product. Future studies should look at improving the reliability of the classification results and the possibility of using other classification techniques to classify a higher number of vegetation classes.

References

- [1] L. Tevdoradze, 'The amount of visitors to mountain resorts during the winter season exceeded 500,000', *FactCheck (Georgia)*, May 15, 2018. https://factcheck.ge/en/story/35551-the-amount-of-visitors-to-mountain-resorts-during-the-winter-season-exceeded-500-000#_ftnref1 (accessed Apr. 06, 2020).
- [2] G. Nakhutsrishvili, O. Abdaladze, K. Batsatsashvili, E. Spehn, and C. Körner, *Plant Diversity in the Central Great Caucasus: A Quantitative Assessment*. Springer International Publishing, 2017.
- [3] D. Marshall Lang and R. Grigor Suny, 'Georgia', *Encyclopædia Britannica*. Sep. 10, 2019, Accessed: Apr. 06, 2020. [Online]. Available: <https://www.britannica.com/place/Georgia>.
- [4] G. Nakhutsrishvili, *The Vegetation of Georgia (South Caucasus)*, vol. 15. Springer-Verlag Berlin Heidelberg, 2013.
- [5] C. Körner and J. Paulsen, 'A world-wide study of high altitude treeline temperatures', *Journal of Biogeography*, vol. 31, no. 5, pp. 713–732, 2004, doi: 10.1111/j.1365-2699.2003.01043.x.
- [6] N. Berdzenishvili and B. Beridzishvili, 'Articles and Statements UDC 33 Svaneti-Ancient Historical and Geographical Province', *Tourism Education Studies and Practice*, vol. 8, no. 2, pp. 39–43, 2016, doi: 10.13187/tesp.2016.8.39.
- [7] SilviFuture, 'Spruce (Oriental)', *Tree Species*, 2014. www.silvifuture.org.uk/species.php?species=65.
- [8] Valen1988, 'Altindere Valley National Park', *Northern Anatolian conifer and deciduous forests*, 2019. en.wikipedia.org/wiki/Northern_Anatolian_conifer_and_deciduous_forests.
- [9] E. Bergmeier, H. Walentowski, and C. Güngöroğlu, 'Turkish Forest Habitat Types – An Annotated Conspectus Based on the EU Habitats Directive with Suggestions for an Upgrade', 2019, pp. 134–292.
- [10] National Park Service, 'The Subalpine Ecosystem', *Rocky Mountain National Park*, 2007. <https://web.archive.org/web/20070809001440/http://www.nps.gov/archive/romo/resources/plantsandanimals/ecosystem/subalpine.html>.
- [11] C. Körner, *Alpine Treelines*, 1st ed. Basel: Springer Basel, 2012.
- [12] M. Caccianiga, C. Andreis, S. Armiraglio, G. Leonelli, M. Pelfini, and D. Sala, 'Climate continentality and treeline species distribution in the Alps', *Plant Biosystems - An International Journal Dealing with all Aspects of Plant Biology*, vol. 142, no. 1, pp. 66–78, 2008, doi: 10.1080/11263500701872416.
- [13] S. Cordell, G. Goldstein, P. J. Melcher, and F. C. Meinzer, 'Photosynthesis and Freezing Avoidance in Ohia (*Metrosideros polymorpha*) at Treeline in Hawaii', *Arctic, Antarctic, and Alpine Research*, vol. 32, no. 4, pp. 381–387, 2000, doi: 10.1080/15230430.2000.12003381.
- [14] G. Kernaghan, 'Ectomycorrhizal fungi at tree line in the Canadian Rockies', *Mycorrhiza*, vol. 10, pp. 217–229, 2001, doi: <https://doi.org/10.1007/s005720000083>.
- [15] A. Dolukhanov, 'Forest vegetation of Georgia', *Universal*, 2010.
- [16] R. Pott, *Biotoptypen : schützenswerte Lebensräume Deutschlands und angrenzender Regionen*. Struttgart: Ulmer, 1996.
- [17] A. Dolukhanov, 'Colchic underwood (Current positions in the mountains of the Caucasus, botanical-geographical relations and origin)', *Metsniereba*, 1980.
- [18] F.-K. Holtmeier, *Mountain Timberlines*, 2nd ed., vol. 36. Springer Netherlands, 2009.
- [19] 'Ornamental Plants of Horticulture Value', *Research*, 2020. www.mobort.org/MOBOT/Research/russia/rhododendron.shtml.
- [20] E. Levier, *A travers le Caucasus*. Neuchatel: Attinger Frères, 1894.

- [21] R. Gagnidze, 'Botanical and geographical analysis of the florocoenotic complex of tall herbaceous vegetation of the Caucasus', *Metsniereba*, 1974.
- [22] R. Gagnidze, 'The ecological-coenotic characteristic and analysis of vertical distribution of tall herbaceous species in the Caucasus', *Zametki Sistem Geogr Rastenii Inst Bot AN GSSR*, no. 34, pp. 41–83, 1977.
- [23] M. Cigler, 'Alpinski louky a Mt. Ushba', *Panoramio*, 2015.
www.panoramio.com/photo/124936347.
- [24] H. Kürschner, G. Parolly, and E. Raab-Straube, 'Phytosociological Studies on high mountain plant communities of the Taurus mountains (Turkey)', *Feddes Repertorium*, vol. 3. Snow-patch and meltwater communities, no. 109, pp. 581–616, 1998.
- [25] G. Parolly, 'The High Mountain Vegetation of Turkey - a State of the Art Report, Including a First Annotated Conspectus of the Major Syntaxa', *Tubitak*, vol. 28, pp. 39–63, 2004.
- [26] A. Kolakovskiy, *Plant world of Colchis*. Publishing House of Moscow University, 1961.
- [27] W. Larcher, *Klimastreß im Gebirge — Adaptationstraining und Selektionsfilter für Pflanzen*, vol. 291. VS Verlag für Sozialwissenschaften, 1980.
- [28] W. Larcher, C. Kainmüller, and J. Wagner, 'Survival types of high mountain plants under extreme temperatures', *Flora - Morphology, Distribution, Functional Ecology of Plants*, vol. 205, no. 1, pp. 3–18, 2010, doi: <https://doi.org/10.1016/j.flora.2008.12.005>.
- [29] C. Körner, J. Paulsen, and E. Spehn, 'A definition of mountains and their bioclimatic belts for global comparisons of biodiversity data', *Alp Botany*, vol. 121, no. 73, 2011, doi: <https://doi.org/10.1007/s00035-011-0094-4>.
- [30] A. Dolukhanov, 'Flora and vegetation of subnival landscapes of the Didi Liakhvi River and the Keli uplan (Greater Caucasus)', *Bot Zh*, vol. 54, pp. 1662–1674, 1969.
- [31] 'Triglav Slovenian Alpine Club 25K Map', Planinska zveza Slovenije, Triglav, Slovenia, 2016.
- [32] 'Alpenvereinskarte 14, Dachsteingebirge', Deutscher Alpenverein, Dachstein, Austria, 2012.
- [33] Wielgolaski and D. W. Inouye, 'High latitude climates.', in *Phenology: An integrative environmental science*, vol. 39, Dordrecht, Boston, London' Kluwer Academic Publishers., pp. 175– 194.
- [34] S. Tuhkanen and E. Sjögren, *Climatic parameters and indices in plant geography*. Stockholm: Almqvist & Wiksell International, 1980.
- [35] P. Beck, C. Atzberger, K. A. Hogda, B. Johansen, and A. Skidmore, 'Improved monitoring of vegetation dynamics at very high latitudes: a new method using MODIS NDVI. Remote Sens Environ', *Remote Sensing of Environment* 100 (2006) 3, vol. 100(3), 2006.
- [36] S. Asam *et al.*, 'Relationship between Spatiotemporal Variations of Climate, Snow Cover and Plant Phenology over the Alps—An Earth Observation-Based Analysis', *Remote Sensing*, vol. 10, no. 11, p. 1757, 2018, doi: 10.3390/rs10111757.
- [37] W. Sulzer, 'Remote Sensing Technologies and Applications for Monitoring High Mountain Environments', presented at the IV. Remote Sensing & GIS Symposium, Zonguldak, Oct. 2012, [Online]. Available: https://www.google.co.uk/url?sa=t&rct=j&q=&esrc=s&source=web&cd=2&cad=rja&uact=8&ved=2ahUKEwiHwfu4xN3oAhUipHEKHVBCC4EQFjABegQIAhAB&url=http%3A%2F%2Fuzalcb.org%2Fwp-content%2Fuploads%2F2016%2F11%2F2012_D3_Wolfgang_Sulzer.pdf&usg=AOvVaw2y_yyukS8m3kCZJNfhbcQK.
- [38] R. Colombo *et al.*, 'Phenological monitoring of grassland and larch in the Alps from Terra and Aqua MODIS images', *Italian Journal of Remote Sensing / Rivista Italiana di Telerilevamento*, vol. 43, pp. 83–96, 2011.

- [39] P. Choler, 'Growth response of temperate mountain grasslands to inter-annual variations in snow cover duration', *Biogeosciences*, vol. 12, pp. 3885–3897, 2015, doi: <https://doi.org/10.5194/bg-12-3885-2015>.
- [40] R. Myneni *et al.*, 'Optical remote sensing of vegetation: Modeling, caveats, and algorithms.', *Remote Sensing of Environment*, vol. 51, pp. 169–188, 2008.
- [41] J. Xie *et al.*, 'Relative Influence of Timing and Accumulation of Snow on Alpine Land Surface Phenology', *Journal of Geophysical Research: Biogeosciences*, vol. 123, no. 2, pp. 561–576, 2018, doi: [10.1002/2017JG004099](https://doi.org/10.1002/2017JG004099).
- [42] N. Pepin, R. S. Bradley, H. F. Dias, M. Baraer, and E. B. Caceres, 'Elevation-dependent warming in mountain regions of the world', *Nature Climate Change*, vol. 5, no. 1758–678X, pp. 424–430, 2015, doi: [10.1038/nclimate2563](https://doi.org/10.1038/nclimate2563).
- [43] A. M. Cingolani, D. Renison, M. R. Zak, and M. R. Cabido, 'Mapping vegetation in a heterogeneous mountain rangeland using landsat data: an alternative method to define and classify land-cover units', *Remote Sensing of Environment*, vol. 92, no. 1, pp. 84–97, 2004, doi: <https://doi.org/10.1016/j.rse.2004.05.008>.
- [44] P. Clark, M. Seyfried, and B. Harris, 'Intermountain plant community classification using Landsat TM and SPOT HRV data', *Journal of Range Management*, vol. 54, 2001, doi: [10.2307/4003176](https://doi.org/10.2307/4003176).
- [45] F. Davis, P. Stine, and D. Stoms, 'Distribution and conservation status of coastal sage scrub in Southwestern California', *Journal of Vegetation Science*, vol. 5, pp. 743–756, 1994, doi: [10.2307/3235887](https://doi.org/10.2307/3235887).
- [46] D. Landgrebe, 'Some Fundamentals and Methods for Hyperspectral Image Data Analysis', *Systems and Technologies for Clinical Diagnostics and Drug Discovery II*, vol. 3603, p. 6, 1999.
- [47] M. Govender, K. Chetty, and H. Bulcock, 'A review of hyperspectral remote sensing and its application in vegetation and water resource studies', *Water S.A.*, vol. 33, 2007, doi: [10.4314/wsa.v33i2.49049](https://doi.org/10.4314/wsa.v33i2.49049).
- [48] N. A. Hagen and M. W. Kudenov, 'Review of snapshot spectral imaging technologies', *Optical Engineering*, vol. 52, no. 9, pp. 1 – 23, 2013, doi: [10.1117/1.OE.52.9.090901](https://doi.org/10.1117/1.OE.52.9.090901).
- [49] C. Iovan, D. Boldo, M. Cord, and M. Erikson, 'Automatic Extraction and Classification of Vegetation Areas from High Resolution Images in Urban Areas', in *Image Analysis*, Berlin, Heidelberg, 2007, pp. 858–867.
- [50] Y. Liu, W. Gong, X. Hu, and J. Gong, 'Forest Type Identification with Random Forest Using Sentinel-1A, Sentinel-2A, Multi-Temporal Landsat-8 and DEM Data', *Remote Sensing*, vol. 10, p. 946, 2018, doi: [doi:10.3390/rs10060946](https://doi.org/10.3390/rs10060946).
- [51] J. Xue and B. Su, 'Significant Remote Sensing Vegetation Indices: A Review of Developments and Applications', *Journal of Sensors*, vol. 2017, no. Article ID 1353691, p. 17, May 2017, doi: [10.1155/2017/1353691](https://doi.org/10.1155/2017/1353691).
- [52] Y. Xie, Z. Sha, and M. Yu, 'Remote sensing imagery in vegetation mapping: a review', *Journal of Plant Ecology*, vol. 1, no. 1, pp. 9–23, 2008, doi: [10.1093/jpe/rtm005](https://doi.org/10.1093/jpe/rtm005).
- [53] S. Vanonckelen, S. Lhermitte, and A. [Van Rompaey, 'The effect of atmospheric and topographic correction on pixel-based image composites: Improved forest cover detection in mountain environments', *International Journal of Applied Earth Observation and Geoinformation*, vol. 35, pp. 320–328, 2015, doi: <https://doi.org/10.1016/j.jag.2014.10.006>.
- [54] G. M. Foody and A. Mathur, 'Toward intelligent training of supervised image classifications: directing training data acquisition for SVM classification', *Remote Sensing of Environment*, vol. 93, no. 1, pp. 107–117, 2004, doi: <https://doi.org/10.1016/j.rse.2004.06.017>.
- [55] C. Alcantara, T. Kuemmerle, A. V. Prishchepov, and V. C. Radeloff, 'Mapping abandoned agriculture with multi-temporal MODIS satellite data', *Remote Sensing of Environment*, vol. 124, pp. 334–347, 2012, doi: <https://doi.org/10.1016/j.rse.2012.05.019>.

- [56] C. Huang, L. S. Davis, and J. R. G. Townshend, 'An assessment of support vector machines for land cover classification', *International Journal of Remote Sensing*, vol. 23, no. 4, pp. 725–749, 2002, doi: 10.1080/01431160110040323.
- [57] M. Pal and P. M. Mather, 'Support vector machines for classification in remote sensing', *International Journal of Remote Sensing*, vol. 26, no. 5, pp. 1007–1011, 2005, doi: 10.1080/01431160512331314083.
- [58] Q. Guo, M. Kelly, and C. H. Graham, 'Support vector machines for predicting distribution of Sudden Oak Death in California', *Ecological Modelling*, vol. 182, no. 1, pp. 75–90, 2005, doi: <https://doi.org/10.1016/j.ecolmodel.2004.07.012>.
- [59] B. Dixon and N. Candade, 'Multispectral landuse classification using neural networks and support vector machines: one or the other, or both?', *International Journal of Remote Sensing*, vol. 29, no. 4, pp. 1185–1206, 2008, doi: 10.1080/01431160701294661.
- [60] J. Knorn, A. Rabe, V. C. Radeloff, T. Kuemmerle, J. Kozak, and P. Hostert, 'Land cover mapping of large areas using chain classification of neighboring Landsat satellite images', *Remote Sensing of Environment*, vol. 113, no. 5, pp. 957–964, 2009, doi: <https://doi.org/10.1016/j.rse.2009.01.010>.
- [61] L. A. Vega Ishuaylas, Y. Hirata, L. C. Ventura Santos, and N. Serrudo Torobeo, 'Natural Forest Mapping in the Andes (Peru): A Comparison of the Performance of Machine-Learning Algorithms', *Remote Sensing*, vol. 10, no. 5, p. 782, 2018, doi: 10.3390/rs10050782.
- [62] D. Lu and Q. Weng, 'A survey of image classification methods and techniques for improving classification performance', *International Journal of Remote Sensing*, vol. 28, no. 5, pp. 823–870, 2007, doi: 10.1080/01431160600746456.
- [63] L. Breiman, 'Random Forests', *Machine Learning*, vol. 45, pp. 5–32, 2001, doi: <https://doi.org/10.1023/A:1010933404324>.
- [64] C. Cortes and V. Vapnik, 'Support-vector networks.', *Machine Learning*, vol. 20, 1995, doi: <https://doi.org/10.1007/BF00994018>.
- [65] G. P. Petropoulos, C. Kalaitzidis, and K. P. Vadrevu, 'Support vector machines and object-based classification for obtaining land-use/cover cartography from Hyperion hyperspectral imagery', *Computers & Geosciences*, vol. 41, pp. 99–107, 2012, doi: <https://doi.org/10.1016/j.cageo.2011.08.019>.
- [66] R. Haapanen, A. R. Ek, M. E. Bauer, and A. O. Finley, 'Delineation of forest/nonforest land use classes using nearest neighbor methods', *Remote Sensing of Environment*, vol. 89, no. 3, pp. 265–271, 2004, doi: <https://doi.org/10.1016/j.rse.2003.10.002>.
- [67] H. Franco-Lopez, A. Ek, and M. Bauer, 'Estimation and mapping of forest stand density, volume, and cover type using the k-nearest neighbors method', *Remote Sensing of Environment*, vol. 77, pp. 251–274, 2001, doi: 10.1016/S0034-4257(01)00209-7.
- [68] R. E. McRoberts, M. D. Nelson, and D. G. Wendt, 'Stratified estimation of forest area using satellite imagery, inventory data, and the k-nearest neighbors technique', *Remote Sensing of Environment*, vol. 82, pp. 457–468, 2002.
- [69] M. Xu, P. Watanachaturaporn, P. K. Varshney, and M. Arora, 'Decision tree regression for soft classification of remote sensing data', *Remote Sensing of Environment*, vol. 97, pp. 322–336, 2005, doi: 10.1016/j.rse.2005.05.008.
- [70] Y. Sohn and N. Rebello, 'Supervised and Unsupervised Spectral Angle Classifiers', *Photogrammetric Engineering and Remote Sensing*, vol. 68, 2002.
- [71] P. Sisodia, V. Tiwari, and A. Kumar, 'Analysis of Supervised Maximum Likelihood Classification for remote sensing image', *International Conference on Recent Advances and Innovations in Engineering, ICRAIE 2014*, 2014, doi: 10.1109/ICRAIE.2014.6909319.
- [72] J. R. Landis and G. G. Koch, 'The measurement of observer agreement for categorical data', *Biometrics*, vol. 33, no. 1, pp. 159–174, 1977, doi: 10.2307/2529310.

- [73] J. A. Hanley and B. Mcneil, 'The Meaning and Use of the Area Under a Receiver Operating Characteristic (ROC) Curve', *Radiology*, vol. 143, pp. 29–36, 1982, doi: 10.1148/radiology.143.1.7063747.
- [74] M. Friedman, 'The Use of Ranks to Avoid the Assumption of Normality Implicit in the Analysis of Variance', *Journal of the American Statistical Association*, vol. 32, no. 200, pp. 675–701, 1937, doi: 10.1080/01621459.1937.10503522.
- [75] G. M. Foody, D. S. Boyd, and C. Sanchez-Hernandez, 'Mapping a specific class with an ensemble of classifiers', *International Journal of Remote Sensing*, vol. 28, no. 8, pp. 1733–1746, 2007, doi: 10.1080/01431160600962566.
- [76] European Space Agency, 'Sentinel-2', *Sentinel Online*, 2020 2000.
<https://sentinel.esa.int/web/sentinel/missions/sentinel-2>.
- [77] European Space Agency, 'Facts and Figures', ESA.
http://www.esa.int/Applications/Observing_the_Earth/Copernicus/Sentinel-2/Facts_and_figures.
- [78] NASA, 'Landsat 8 Overview', *Landsat Science*, 2020. <https://landsat.gsfc.nasa.gov/landsat-8/landsat-8-overview/>.
- [79] R. B. Smith, 'Introduction to hyperspectral imaging', *MicroImages*, 2001, Accessed: Aug. 22, 2020. [Online]. Available: www.microimages.com.
- [80] Mapasyst, 'Remote Sensing Resampling Methods', *Geospatial Technology*, Aug. 21, 2019.
<https://mapasyst.extension.org/remote-sensing-resampling-methods/#:~:text=Nearest%20neighbor%20is%20a%20resampling,values%20in%20the%20unaltered%20scene>. (accessed Sep. 08, 2020).
- [81] R. Geerken, B. Zaitchik, and J. Evans, 'Classifying rangeland vegetation type and coverage from NDVI time series using Fourier Filtered Cycle Similarity', *International Journal of Remote Sensing*, vol. 26, pp. 5535–5554, Feb. 2005, doi: <https://doi.org/10.1080/01431160500300297>.
- [82] J. A. Richards, *Remote Sensing Digital Image Analysis*. Berlin: Springer-Verlag, 1999.
- [83] 'Past Weather in Tbilisi Georgia', *timeanddate.com*, 2020. www.timeanddate.com.
- [84] D. Chen*, D. A. Stow, and P. Gong, 'Examining the effect of spatial resolution and texture window size on classification accuracy: an urban environment case', *International Journal of Remote Sensing*, vol. 25, no. 11, pp. 2177–2192, 2004, doi: 10.1080/01431160310001618464.
- [85] B. L. Markham and J. R. G. Townshend, 'Land cover classification accuracy as a function of sensor spatial resolution.', in *Proceedings of the 15th International Symposium on Remote Sensing of Environment*, Ann Arbor: ERIM, 1981, pp. 1075–1090.
- [86] M. Vanhellemont, J. V. Acker, and K. Verheyen, 'Exploring life growth patterns in birch (*Betula pendula*)', *Scandinavian Journal of Forest Research*, vol. 31, no. 6, pp. 561–567, 2016, doi: 10.1080/02827581.2016.1141978.